International
Progress Report

IPR-07-22

Äspö Hard Rock Laboratory

Prototype Repository

THM modelling of the bentonite buffer

Canister mid-height 1D radial models, holes #1 and #3

Ola Kristensson
Harald Hökmark

Svensk Kärnbränslehantering AB

January 2010

Svensk Kärnbränslehantering AB
Swedish Nuclear Fuel
and Waste Management Co

Box 250, SE-101 24 Stockholm
Phone +46 8 459 84 00

Äspö Hard Rock
Laboratory

Report no.
IPR-07-22

No.
KBP1001

Author
Ola Kristensson
Harald Hökmark

Date
January 2010

Checked by
Anders Sjöland

Date
July 2011

Approved
Mats Ohlsson

Date
September 2011

Äspö Hard Rock Laboratory

Prototype Repository

THM modelling of the bentonite buffer

Canister mid-height 1D radial models, holes #1 and #3

Ola Kristensson

Harald Hökmark

January 2010

Keywords: Prototype Repositoty, THM modelling, Thermal process, Water saturation, Homogenization

Executive summary

In SKI's statement concerning SKB's Research-Development-Demonstration (FUD) program 2004, /SKI, 2005/, SKI called attention to that there was a necessity to prove the adequacy of the knowledge and the numerical tools in the context of the engineered buffer by performing comparisons between experiments and models. The finite element code Code_Bright was also considered to be very promising when interpreting the Prototype Repository. SKI also pointed out that understanding of the homogenization and other processes in the slots in the engineered buffer are of importance.

The main objective of this report is to perform numerical studies of the thermal process, water saturation process and the homogenization of the engineered buffer in the Prototype Repository experiment. A coupled Thermal (T), hydrologic (H) and mechanical (M) radial-symmetric 1D-problem is solved by using the finite element program Code_Bright, /CIMNE, 2004/.

The model is a representation of the engineered buffer system between the canister and the rock wall at canister mid-height, see Figure 1. There are three different sections between canister and rock wall. The main part consists of bentonite powder compressed into blocks (2). There is a slot between the block and the rock wall that is filled with bentonite pellets (3). The individual pellets also consist of compressed bentonite powder. Initially there is a difference between block and pellet slot density. Initially there is also an open slot between canister and bentonite block (1). When the buffer takes up water, the inner slot will close and the density difference between block and pellet slot will start to decrease.

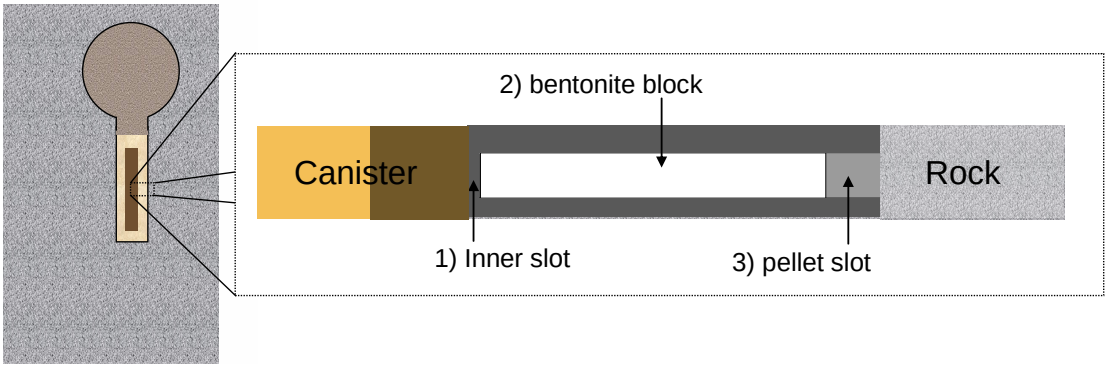

Figure 1 ***Schematic picture of the buffer section analyzed in this work.***

The pellet slot thermal conductivity is evaluated using temperatures measured at different radial distances in the buffer. The value 0.29 W/(m·K) is considered the best estimate of the initial pellet slot thermal conductivity.

The canister heat flux at canister mid-height is used as one of the thermal boundary conditions in the model. This variable is obtained from the thermal 3D-model described in /Kristensson and Hökmark, 2007/. To validate if the canister heat flux is representative, the obtained bentonite block conductivity, calculated using measured block temperatures and the simulated heat flux, is compared with experimental values. The comparison indicates that the model and experimental heat fluxes for canister #1agree and that the heat flux of canister #3 is somewhat overestimated by the simulation.

In order to capture the homogenization process a valid representation of the pellets-filled outer slot is of importance. Here the pellet slot is homogeneously represented, .i.e. the individual pellets are not considered. A method using the radial void ratio profile, observed in

the Canister Retrieval Test (CRT) at full water saturation /Johannesson, 2007/, and the measured stress history in hole #1 when calibrating the mechanical properties for the homogenized pellet slot is evaluated. The method produces results that are in agreement with the experimental findings.

Direct comparisons between measured and calculated histories of temperature, suction and stress at different radial distances give reasonable agreement. The overall character of the responses is captured with the model. Some of the discrepancies are listed in the following.

- The temperatures are slightly underestimated by the model.
- The initial drying process recorded at the sensor position closest to the canister is only captured using the model where the mechanics is excluded.

Adjusting some parameter in the models could eliminate the discrepancies, but here the approach was that parameter values based on laboratory data should not be altered.

The general validity of the developed model is investigated by analyzing two different holes, hole #1 and hole #3, which have different water inflows. Hole #1 is categorized as wet and hole #3 as dry, /Rhén and Forsmark, 2001/. The difference of the models corresponding to the different holes is expressed by using different boundary conditions, i.e. the same set of material parameters is used for modeling both holes.

The strength of the coupling of the TH evolution to the mechanical process is studied by analyzing model versions with the only difference being incorporating the mechanical logic or not. The temperature appears to be insignificantly dependent on the mechanical processes, whereas the hydraulic response depends strongly on the mechanical processes. The water saturation process is slowed down when incorporating the mechanics.

This study also serves as a general investigation of the applicability of the numerical tool, Code_Bright, to this type of analysis. It is found that the tool provides possibilities that are very useful when interpreting the Prototype Repository experiment.

Sammanfattning

I SKI's yttrande över SKB's Forsknings –Utvecklings- och Demonstrationsprogram (FUD) 2004, påtalade SKI att det fanns ett behov att visa, genom att göra jämföresler mellan experiment och modeller, att kunskapen och de numeriska verktyg som används i samband med studier av ingenjörsbarriärer är ändamålsenliga. Det finita elementprogrammet Code_Bright ansågs lovande för tolkning av Prototypförvaret. SKI pekade också på att förståelsen av homogeniseringsprocessen och andra processer i ingenjörsbarriärens spalter är betydelsefull.

Syftet med denna rapport är att genomföra numeriska studier av den termiska processen, vattenmättnadsprocessen och homogenisersigsprocessen i ingenjörsbarriären i Prototypförvaret. Ett kopplat Termiskt (T), hydrauliskt (H) och Mekansikt (M) radialsymmetriskt 1-D problem löses med användning av det finita elementprogrammet Code_Bright /CIMNE, 2004/.

Modellen representerar ingenjörsbarriären mellan kapseln och begväggen vid kapselns höjdcentrum, se Figure 1. Det finns tre sektioner mellan kapsel och bergvägg. Huvuddelen består av block pressade av bentonitpulver (2). Det finns en spalt, fylld med bentonitpellets, mellan block och bergvägg (3). De individuella pelletsen är också pressade av bentonitpulver. Initialt finns det en densitetsskillnad mellan blocken och den pelletsfyllda spalten. Initialt finns det också en en öppen, inre, spalt mellan kapsel och block (1). När bufferten tar upp vatten börjar den inre spalten slutas samtidigt som, på grund av bentonitens utsvällning, densitetsskillnaden mellan block och pelletsspalt börjar minska.

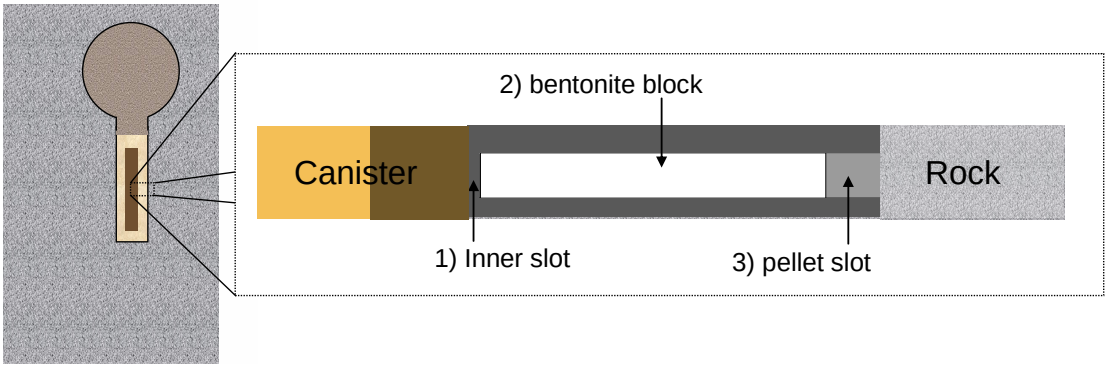

Figure 1 ***Schematsk bild av buffertsektionen som analyseras i detta arbete.***

Den termiska konduktiviteten i pelletsspalten utvärderas utifrån temperaturer uppmätta på olika radiella avstånd i bufferten. Värdet 0.29 W/(m·K) bedöms vara det bästa värdet för pellestsspaltens termiska konduktivitet.

Kapselytans värmeflödestäthet vid kapselns höjdcentrum används som randvillkor i modellen. Värde på denna variabel erhålls från den termiska 3D modellen i /Kristensson och Hökmark, 2007/. För att bekräfta giltigheten av det antagna termiska flödet jämförs den termiska värmeledningsförmåga man kan beräkna ur flödet och de uppmätta temperaturerna i bufferten med experimentellt bestämda buffertvärmeledningstal. Jämförelsen inidikerar att värmeflödet hos kapsel #1 stämmer väl, medan det för kapsel #3 överskattas något i simuleringen.

För att i modellen återskapa densitetsutjämnningsprocessen är en välgrundad representation av pelletsspalten betydelsefull. Här är spalten homogent representerad, dvs de enskilda pelletsarna beaktas inte. Mätningar av den radiella portalsprofilen vid full vattenmättnad i

Återtagsförsöket (CRT) i Äspölaboratoriet används för att ta fram och kalibrera parametervärden till de mekaniska egenskaperna i den homogena spalten.

Direkta jämförelser mellan den beräknade och experimentellt bestämda utvecklingen av temperatur, relativ fuktighet och spänning på olika radiella avstånd från kapselytan ger rimliga överenstämmelser. Den allmänna karaktären hos den experimentellt utvecklingen återskapas i modellen. Några avvikelser finns:

- Temperaturerna underskattas något i modellen
- Den initiella uttorkning som registrerades i givarpostionerna närmast kapseln återskapas bara i den modeller där mekaniken inte beaktas.

Avvikelserna skulle i någon mån kunna elimineras genom att justera några av parametervärdena, men här var avsikten att inte ändra laboratoriebestämda parametervärden.

Den här utvecklade modellens allmänna giltighet kontrolleras genom att analysera två deponeringshål, hål #1 och hål #3, med olika vattenflöden. Hål #1 betraktas som vått och hål #3 som torrt /Rhen och Forsmark, 2001/. Skillnaderna mellan de två modellerna har bara med de olika randvillkoren att göra, dvs samma parameteruppsättning och samma parametervärden används i båda modellerna.

Styrkan av kopplingen av den termo-hydrauliska utvecklingen till den mekaniska processen undersöks genom att analysera modellerversioner som bara skiljer sig åt genom att den mekaniska logiken är inkopplad eller urkopplad. Temperaturen visar sig vara i stort sett oberoende av den mekaniska utvecklingen, medan vattenmättnadsprocessen bromsas när mekaniken kopplas in.

Studien fungerar också som en allmän undersökning av det numerisk verktygets, Code_Bights, allmänna tillämplighet vid den här typen av studier. För tolkning av Prototypförvaret visar sig Code_Bright tillhandahålla flera användbara möjligheter.

Contents

1 Introduction 9
1.1 General 9
1.2 Scope and objectives 10

2 Modeling approach 13
2.1 General 13
2.2 Realization 13

3 Model description 15
3.1 Initial conditions 15
3.1.1 Thermal initial conditions 16
3.1.2 Hydraulic initial conditions 16
3.1.3 Mechanical initial conditions 17
3.2 Constitutive laws and parameter values 17
3.2.1 Conductive heat transfer 18
3.2.2 Water retention 25
3.2.3 Liquid water flow 28
3.2.4 Vapor diffusion 29
3.2.5 Mechanical behavior 30
3.3 Boundary conditions 32
3.3.1 Thermal boundary conditions 33
3.3.2 Hydraulic boundary conditions 39
3.3.3 Mechanical boundary conditions 40
3.4 Model overview 40

4 Results and discussion 41
4.1 Mesh dependence 41
4.2 Hole #1 (wet conditions) 43
4.2.1 Thermal response 44
4.2.2 Hydraulic response 48
4.2.3 Mechanical response 56
4.3 Hole #3 (dry conditions) 59
4.3.1 Thermal response 60
4.3.2 Hydraulic response 61
4.3.3 Mechanical response 63

5 Conclusions and comments 65
5.1 Model generality 65
5.2 Dependency on homogenization and porosity 66
5.3 Thermal response 67
5.4 Hydraulic response 67
5.5 Mechanical response 68
5.6 Future work 68

6 References 69

Appendix A - Calculating the suction rate 71

1 Introduction

1.1 General

The Prototype Repository Project simulates a part of a KBS-3 nuclear waste repository /Börgesson et al., 2002/. Within the Prototype Repository project the performance of such a repository during the first years after deposition can be tested on the 50 m scale. The behavior of the system is monitored by use of numerous instruments of different types positioned in the near-field rock, in the electrically heated canisters and in the bentonite buffer. The Prototype Repository also offers a great possibility to investigate to what extent models agree with reality.

Figure 1-1 shows the geometry of the experiment and in Table 1-1 some geometrical data is shown. The Prototype Repository consists of two sections. The first, inner, section contains four full-scale deposition holes, each with a canister and a surrounding bentonite buffer, while the second, outer, section contains two such holes. The tunnel and the 1 m top parts of the deposition holes are filled with backfill material, consisting of bentonite and crushed rock. The sections are separated by a concrete plug to allow for separate dismantling and different test times. There is an additional outer plug to confine the experiment mechanically and hydraulically and to simulate the conditions near a seal in a real repository. To simulate the thermal behavior of the nuclear waste, heaters are installed in the canisters.

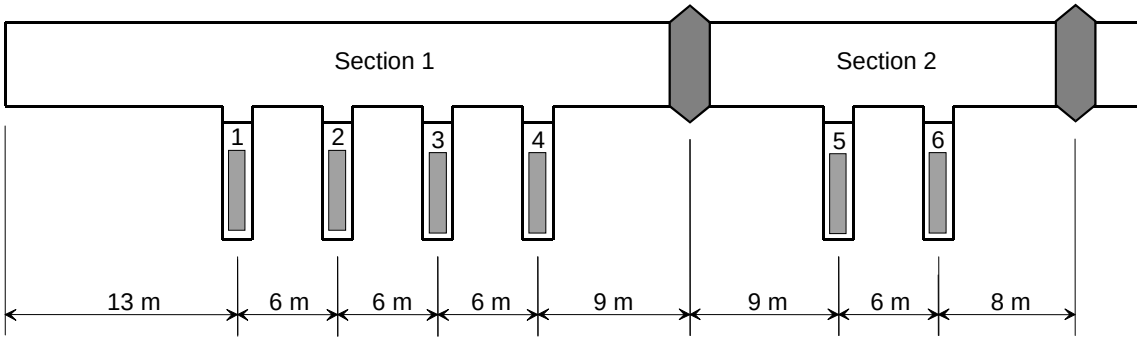

Figure 1-1 ***Geometry of the Prototype Repository.***

Table 1-1 ***Geometric data of the Prototype Repository.***

Deposition hole depth	8 m	Bentonite thickness above the canister	1,5 m
Deposition hole diameter	1,75 m	Total tunnel length	63 m
Canister height	~5 m	Length of section I	40 m
Canister diameter	1,05 m	Length of section II	23 m
Bentonite thickness below the canister	0,5 m	Tunnel diameter	5 m

In /Kristensson and Hökmark, 2007/, 3-D simulations of the temperature evolution in Prototype Repository rock mass are described. In the 3-D thermal models, the rock thermal conductivity is represented by one global value or by two different values, one in the tunnel floor and another in the remaining rock mass. The measured temperature evolution in the pillars between the deposition holes was well captured using this simple representation of the rock conductivity. The agreement between model and measurement verifies the input power history of the six canisters.

In the present work 1-D radial THM models are developed to simulate the behavior of the buffer at canister mid-height in holes #1 and #3. The thermal input (canister power and rock temperature) is obtained from the thermal 3-D model in /Kristensson and Hökmark 2007/.

1.2 Scope and objectives

The focus is on the engineered buffer system between the canister and the host rock wall at canister mid-height, see Figure 1-2. There are three different sections between the canister and rock wall:

1. Initially there is an open slot between the canister and the bentonite blocks

2. The main part consists of bentonite powder compressed into blocks.

3. There is a slot between the block and the rock wall filled with bentonite pellets

The individual pellets also consist of compressed bentonite powder. There is an initial density difference between the block and the pellet slot. When the buffer takes up water from the surrounding rock, the inner slot will start to close and the density in the block and pellet slot will homogenize due to swelling.

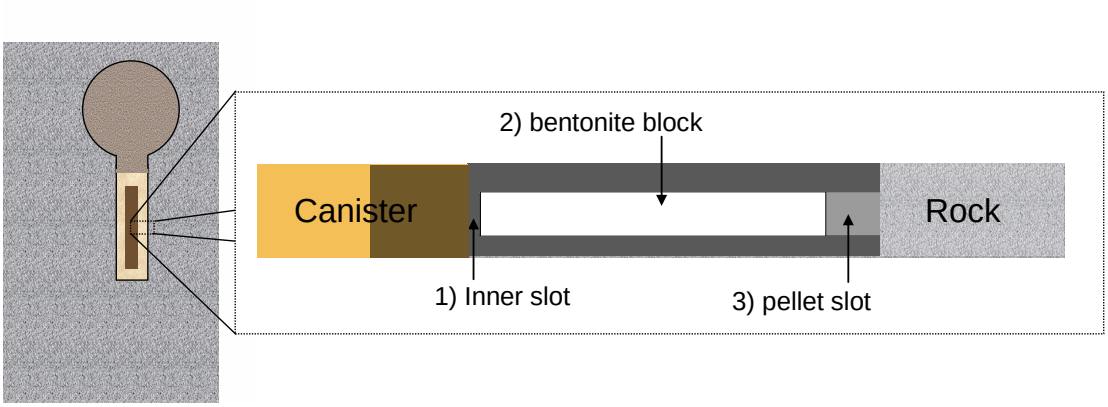

Figure 1-2 ***Schematic picture of the buffer section analyzed in this work.***

The main topics of the investigation are the water saturation process and the homogenization of the buffer. Thermal (T), hydrologic (H) and mechanical (M) conditions and processes are considered in this numerical study by using the finite element program Code_Bright, /CIMNE, 2004/.

The general validity of the developed model is investigated by modeling two different holes, hole #1 and hole #3, which have different water inflows. Based on inflow measurements conducted before installation, hole #1 is characterized as wet and hole #3 as dry, see /Rhén and Forsmark, 2001/. The difference of the models corresponding to the different holes is expressed by using different boundary conditions. The same set of material parameter values is used for both holes

To capture the homogenization process, a valid representation of the pellet filled outer slot is an important issue. The pellet slot is homogeneously represented, i.e. the individual pellets are not considered. The radial void ratio profile found at full water saturation in the Canister Retrieval Test (CRT) /Johannesson, 2007/, was used together with the measured stress history in hole #1 to calibrate the mechanical properties of the homogenized pellet slot.

The strength of the coupling of the TH responses to the mechanical process is studied. The effect of considering explicit porosity dependence of retention and permeability on the THM response is investigated as well.

This study also serves as a general investigation of the applicability of the used numerical tool, Code_Bright, in this field of application.

2 Modeling approach

2.1 General

This study is performed using the finite element program Code_Bright, /CIMNE, 2004/. Code_Bright is, together with Abaqus, presently one of the SKB reference tools for modeling THM processes in the repository buffer.

Variations in bentonite properties are considered to be small. Identical tests with samples taken from different material deliveries give equivalent results. Since the same technique for production of bentonite blocks and pellets was used for the material both holes considered here (#1 and #3), the differences in response between the two holes are due only to differences in thermal and hydrological boundary conditions. This means that different deposition holes should be analysed using identical material models. This is, however, possible only if the buffer material model is capable of representing the system under the different conditions that will prevail due to differences in the boundary conditions. Here it is implicitly assumed that this is the case, i.e. that the selected material laws and the selected model parameter values are valid within wide enough ranges of, for instance, water saturation, that relevant comparisons can be made between results obtained for the two holes.

Here, the pellet-filled slot is assumed to be homogenized from the start, i.e. considered as a low density bentonite block with a homogenized density. The block-slot density difference is very significant, and it appears that the material model is not sufficiently general to cover the THM behavior of both materials with one set of model parameter values. Therefore, a specific slot model is defined with parameter values being calibrated from results of a similar field test. Similar to the block model, the slot model is the same for the two holes.

2.2 Realization

Where available, parameter values obtained from laboratory experiments are used. Otherwise a manual fitting of the parameters, so that the solutions correspond well with the recorded, is used.

The bentonite block properties have mostly been obtained from laboratory experiments. For the pellet slot mechanical parameters, which have not been determined independently in laboratory experiments, the parameters are adjusted so to obtain a qualitative fit between a radial void ratio profile of the Canister Retrieval Test (CRT), obtained after dismantling the experiment /Johannesson, 2007/, and the simulated radial void ratio profile at full water saturation. A fitting to the measured stress history in hole #1 has also been used when calibrating the pellet slot parameters.

Simulations of the different holes, hole #1 (with wet conditions) and hole #3 (with dry conditions), are modeled by prescribing different thermal and hydraulic conditions. The hole-specific thermal conditions, i.e. the canister heat flux and the rock wall temperature, are obtained from a thermal 3D simulation where the whole Prototype Repository experiment geometry is included, see /Kristensson and Hökmark, 2007/. The hole-specific hydraulic conditions are controlled by specifying the initial water saturation of the inner slot between canister and bentonite block, and by controlling the water influx at the rock wall with a leakage coefficient and an applied rock wall water pressure.

Incorporating the leakage coefficient, when specifying the hydraulic boundary condition at the rock wall boundary, is a way to represent the hole-specific hydraulic properties of the near-field rock without actually modeling that rock and without attempting to describe the temporal evolution of the liquid pressure at the boundary. The leakage coefficient is

calibrated so that the suction response closest to the rock is similar between experiment and simulation for the period of time considered here..

3 Model description

In this section a description of the model is given. The geometry, constitutive laws, parameter values are shown and the boundary conditions are discussed in general. In following sections detailed motivations and discussions of the parameters, initial conditions and boundary conditions are given.

A continuum description of the problem has been adopted and Code_Bright, a finite element code developed for handling coupled THM geological problems, see /CIMNE, 2004/, is used for solving the problem. Here, a one dimensional model has been developed, where axisymmetry has been utilized. The geometry of the problem is shown in Figure 3-1, where three different sections can be recognized. The sections are: 1) The slot between the rock and the bentonite block which is filled with bentonite pellets 2) The bentonite block 3) The slot between the bentonite block and the canister.

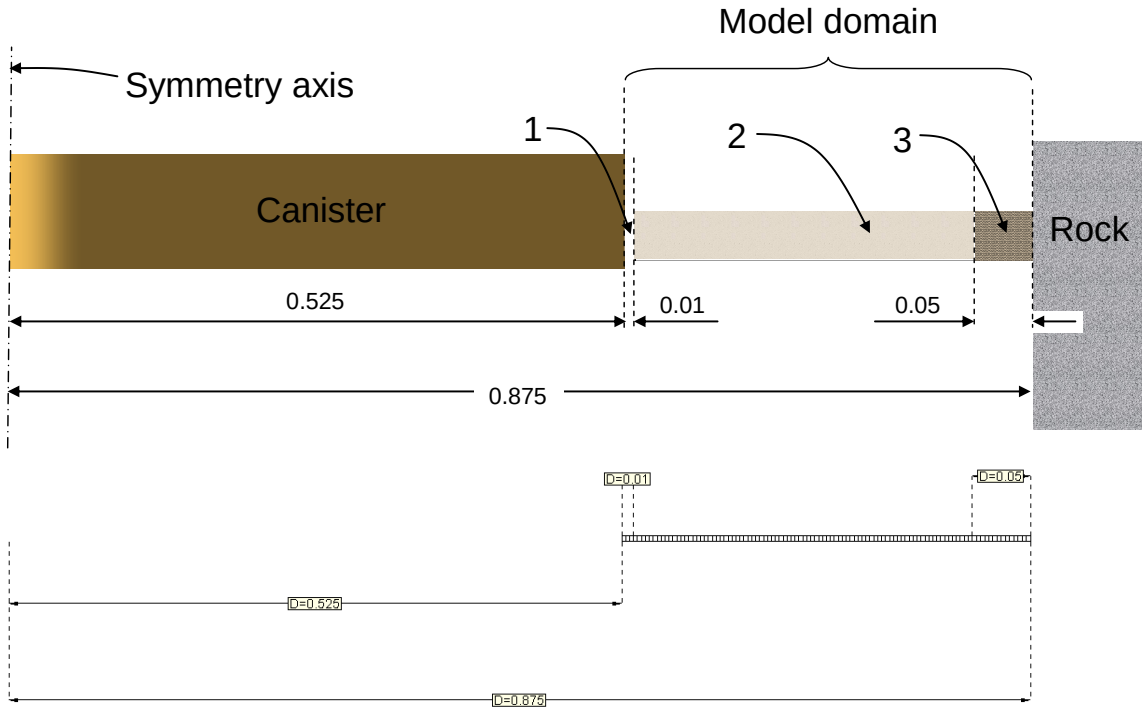

Figure 3-1 ***Schematic geometry (top) and the actual model geometry with the Base Case mesh consisting of 1×103 elements (bottom).***

Figure 3-1 also shows the 1×103 finite element mesh used in the simulations. The quadrilateral elements have linear shape functions and 4 integration points. Also, the elements have a modified **B** matrix (the **B** matrix contains the functions that link the node displacements with the strain tensor) which corresponds to using a selective integration.

3.1 Initial conditions

In this section the initial conditions are shown and discussed. The initial conditions are shown in Table 3-1.

Table 3-1 ***Initial conditions.***

Material	T [°C]	w/S_l	e/n	$\boldsymbol{\sigma}$ [MPa]	p_g [MPa]	p_l [MPa]
Block	15	0.171 / 0.864	0.55 / 0.355	**0**	0.1	-44.93
Pellets		0.13 / 0.239	1.51 / 0.602			-52.01
Inner slot (hole #1)		5.79 / 0.328	49 / 0.98			-0.88
Inner slot (hole #3)		0.018/ 0.001				-45.00

Initial conditions are given in terms of the temperature, T, the water ratio, w, (or the equivalent water saturation, S_l), the void ratio, e, (or the equivalent porosity, n), the total stress tensor, $\boldsymbol{\sigma}$, the gas pressure, p_g, and the liquid pressure, p_l.

3.1.1 Thermal initial conditions

All sections of the model have the same initial temperature of 15 °C.

3.1.2 Hydraulic initial conditions

Bentonite block

The initial water ratio of the bentonite block have been obtained from averaging site data for the first section, i.e. hole #1, #2, #3 and #4, see /Börgesson et al 2002/.

The gas pressure is set to atmospheric. To obtain the initial bentonite block liquid pressure, the suction, $S = p_g - p_l$, is determined using the psychrometric law with values from lab-scale measurements of the relative humidity, RH:

$$S = -\frac{R(273.15+T)\rho_l}{M_w}\ln\left(\frac{RH}{100}\right) \quad (1)$$

Here, R is the universal gas constant, ρ_l the water density and M_w the molecular mass of water. That the suction value that would be obtained from RH readings actually recorded in the experiment is relative high, approximately 55 MPa, as compared to values obtained in laboratory tests, approximately 45 MPa, for the same material. A possible reason for the discrepancy between the field test RH data and laboratory RH data is that the section of bentonite around the sensor has been heterogenic in the field test.

The heterogeneity comes from the installation of the RH sensors, holes were drilled in the bentonite block into which the sensors were fitted. The holes were then backfilled with bentonite powder which had a lower initial water ratio of 0.1 as compared to the bentonite block which had an initial water ratio of 0.171. This is probably the reason for the high initial suction (low initial relative humidity) of the field test as compared to laboratory data. The low field test RH readings are considered to be caused by local installation disturbances and are, consequently, not taken to be representative of conditions on the scale relevant to the modeling.

When modeling the retention of the bentonite, only lab data has been considered, since no heterogeneity due to sensor backfill is incorporated in the model. The initial suction will therefore be underestimated as compared to the one recorded in the field test and a discrepancy between the experimental and simulated suction can therefore be expected.

Pellet slot

With an assumption of no additional water in the slot filled with pellets the homogenized initial water ratio $\overline{w}$ equals that of the individual pellet, i.e. $\overline{w} = w = 0.13$.

Inner slot

The inner slot is represented in the Code_Bright model as air/water with a very small fraction of bentonite. Since the different holes, hole #1 and hole #3, have different hydraulic conditions initially, the former is wet and the latter is dry, different initial slot water ratios have been adopted when modeling the specific holes.

The initial water saturation has been calibrated so that the simulated suction response at the innermost sensor position (at the radial position r = 0.585 m) is in close agreement to the experimental suction response. Using this calibration method, w = 5.79 was found suitable for hole #1 and w = 0.018 was found suitable for hole #3.

3.1.3 Mechanical initial conditions

Bentonite block

The initial void ratio of the bentonite block have been obtained from averaging site data for the first section, i.e. hole #1, 2, 3 and 4, see /Börgesson et al 2002/.

Pellet slot

When it comes to the slot filled with pellets, a homogenized representation has been adopted. The expression in (2) has been used to calculate the homogenized void ratio $\overline{e}$.

$$\overline{e} = \frac{\rho}{\overline{\rho}}(e+1) - 1 \tag{2}$$

A value of $\overline{e} = 1.51$ has been obtained by using the following data:

- The pellet density $\rho = 2.04$ Mg/m^3, obtained from taking the mean value of the minimum and maximum values given in /Börgesson et al 2002/.
- The homogenized pellet density $\overline{\rho} = 1.25$ Mg/m^3 obtained from experimental data.
- The pellet void ratio $e = 0.54$, given by the water ratio $w = 0.13$, the compact density $\rho_s = 2.78$ Mg/m^3, and the pellet density presented above.

Inner slot

Since the inner slot is represented, as mentioned above, as air/water with a very small fraction of bentonite, the void ratio is accordingly prescribed to a large value.

3.2 Constitutive laws and parameter values

Here follows a description of the used constitutive laws together with the ingoing parameter values for the different materials.

Table 3-2 ***Balance law parameter values***

Parameter	Block	Pellets	Slot
ρ_s [kg/m^3]	2780		
c [J/(kg K)]	800		

The values of the solid (or compact) mass density ρ_s and specific heat (for material with the compact density) c are given in Table 3-2.

3.2.1 Conductive heat transfer

Table 3-3 ***Constitutive law of conductive flux of heat and the adopted parameter values***

Constitutive law	Parameter	Block	Pellets	Slot
Conductive heat flux $\boldsymbol{i}_c = -\lambda \nabla T$ $\lambda = \lambda_{sat} S_l + \lambda_{dry}(1 - S_l)$	λ_{dry} [Wm/K]	0.3	0.2	0.06
	λ_{sat} [Wm/K]	1.3	1.1	0.6

$\boldsymbol{i}_c$ is the conductive heat flux, λ the conductivity, ∇T the temperature gradient and S_l the water saturation.

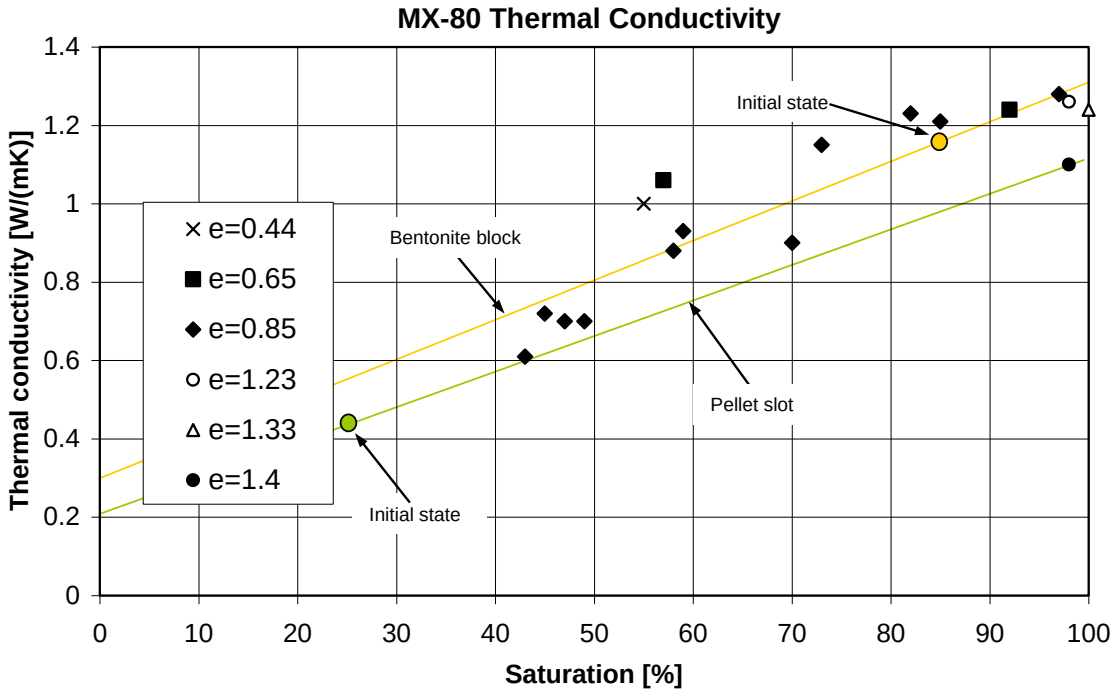

Figure 3-2 ***Heat conductivity of MX80 bentonite as function of the degree of saturation. The legend gives the void ratio. The adopted models for the bentonite block and pellet slot are indicated and also the initial states.***

The parameter values of bentonite block thermal conductivity for dry conditions, λ_{dry}, and saturated conditions, λ_{sat}, have been obtained from studying the average trend of the experimental measurements (from /Börgesson and Hernelind, 1999/) in Figure 3-2, where also the adopted model and the initial state, corresponding to a conductivity of 1.164 W/(m·K), are indicated. If comparing the chosen model with the experimental findings of e = 0.44 and e = 0.65 (the initial void ratio is 0.55 for the bentonite block) the model seems to produce somewhat low values of conductivity. In the relevant water saturation rage (> 85 %), however, the underestimation is not considerable. Figure 3-2 suggests that an initial conductivity of a little more than 1.2 W/(m·K) would be more representative for the initial bentonite block void ratio.

The pellet slot thermal conductivities have been obtained from /Börgesson and Hernelind, 1999/ and /Sugita et al 2003/. Using the initial water saturation in the expression shown in Table 3-3 gives an initial pellet slot conductivity of 0.42 W/(m·K). The model and initial state are shown in Figure 3-2. The pellet slot conductivity is studied further in the following section.

The inner slot dry thermal conductivity has been obtained from /Hökmark and Fälth, 2003/ where a value of the effective thermal conductivity is calculated from considering radiation and conduction processes in the open slot. The heat transfer by radiation has been included in the model in this manner since Code_Bright presently lacks this mechanism. The inner slot thermal conductivity for fully saturated conditions is set equal to the thermal conductivity of water.

Investigation of the pellet slot conductivity

To investigate the thermal conductivity of the pellet slot further, temperature profiles in the buffer at canister mid-height in hole #5 and hole #6 of the prototype repository have been studied. In Figure 3-4 the temperature profiles at several times, measured from the start of the heater in the corresponding hole, (2003-05-08 for hole #5 and 2003-05-23 for hole #6), are presented. The temperatures at r = 0.825 have been calculated using the expression

$$q_r(r_0) r_0 \ln \frac{r_1}{r_2} = -\lambda(r_1, r_2)(T(r_1) - T(r_2)), \tag{3}$$

where q_r is the radial conductive heat flux. An assumption of radial heat flow is suitable close to the canister at canister mid-height. Also making use of an assumption of constant bentonite block conductivity from r = 0.685 m to r = 0.825 m makes it possible to calculate the sought temperature at r = 0.825 m from the experimental temperatures at r = 0.685 m and r = 0.785 m or r = 0.785 m together with their radial position inserted in (3).

The sensor label and position, (z = height above hole floor\$\alpha$ = orientation\$r$ = radial distance from hole center line), for the sensors used in the investigation are shown in Table 3-4 and Table 3-5. The used coordinate system is shown in Figure 3-3.

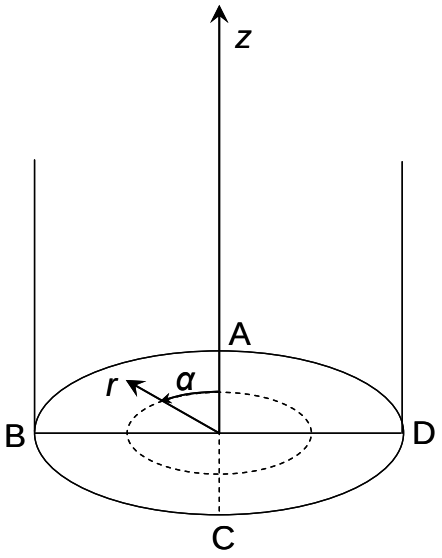

Figure 3-3 ***Coordinate system used for describing the positions of the sensors. z = 0 is at the cement casting in the bottom of the hole, r = 0 is at the hole center line and A is headed against the end of the tunnel.***

Table 3-4 ***Sensor label and position for the sensors used in hole #5 .***

orientation	Sensor label and position ($z\backslash\alpha\backslash r$)			
80° - 85°	TB513 (2.950\85°\0.585)	TB514 (2.950\85°\0.685)	TB515 (2.950\85°\0.785)	TR5055 (3,0\80°\0,875)
170° - 180°	TB516 (2.950\175°\0.585)	TB517 (2.950\175°\0.685)	WB521 (2.750\180°\0.785)	TR5045 (3,0\170°\0,875)

Table 3-5 ***Sensor label and position for the sensors used in hole #6 .***

orientation	Sensor label and position (z = 2.750\ α = 270°\r)						
270°	TB612 r = 0.535	TB613 r = 0.585	TB614 r = 0.635	TB615 r = 0.685	TB616 r = 0.735	TB617 r = 0.785	TB618 r = 0.875

It should be mentioned that the sensor data of TB513(2.950\85°\0.585) and TB514(2.950\85°\0.685) is showing signs of being unreliable in the interval day 315 – day 453 and has been adjusted. In the interval from day 315 – day 453 the data has been linearly interpolated since the temperature instantaneous increases with 1.63 °C and 1.68 °C at day 315 for TB513 and TB514, respectively, and the data then has an instantaneous decrease at day 453.

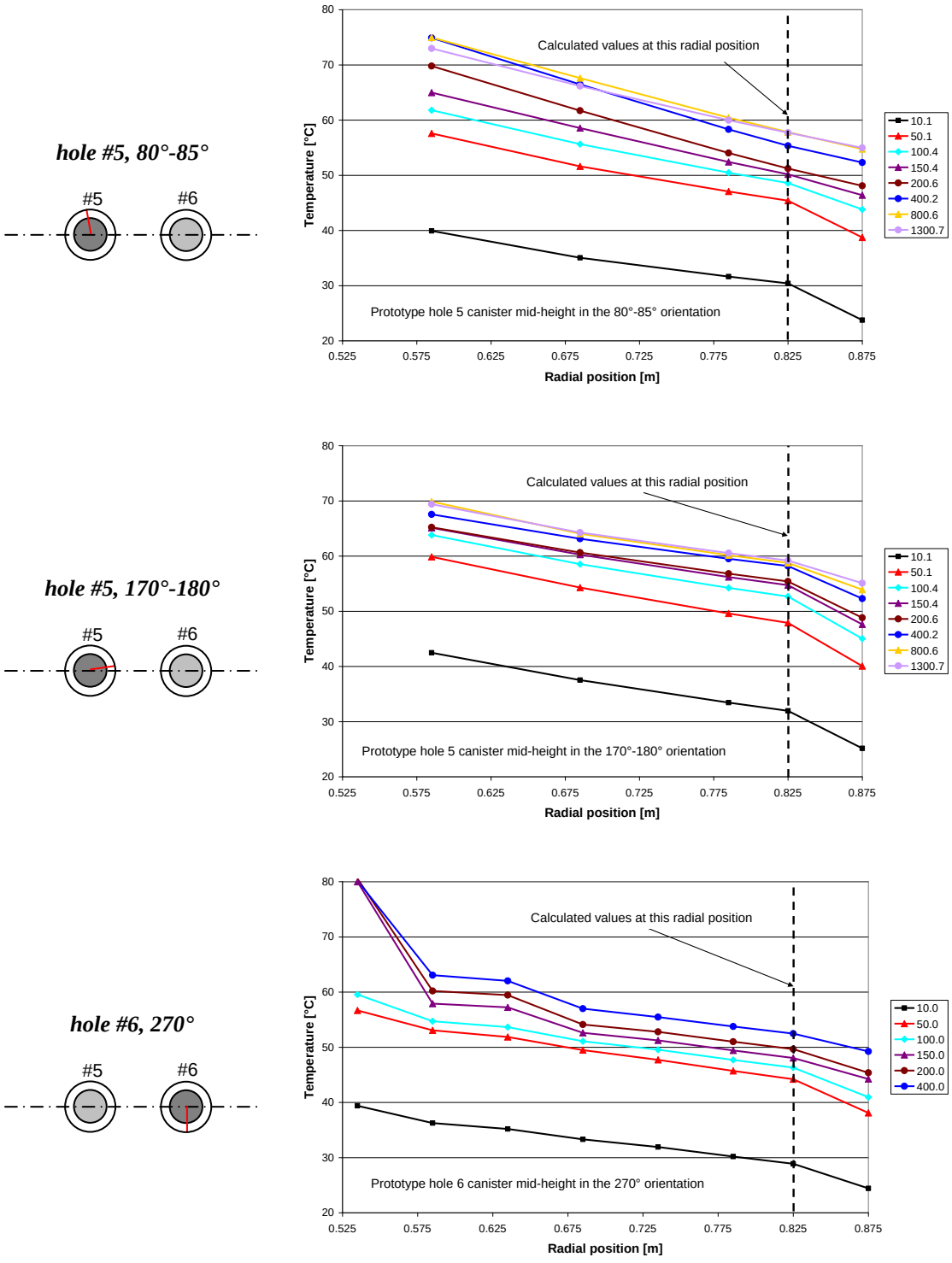

Figure 3-4 ***Temperature profiles in the buffer at canister mid-height in hole #5 in the orientations 80°-85° (top) and 170°-180° (mid) and in hole #6 in the orientation 270° (bottom). The values at r = 0.825 are calculated and the rest are meaured. Note that the time indicates number of days since the heater in the corresponding hole was started (2003-05-08 for hole #5 and 2003-05-23 for hole #6).***

The temperature profiles show that there is a significant difference in temperature gradient in the bentonite block and the pellet slot initially. The larger gradient in the pellet slot indicates that the slot has lower conductivity as compared to the bentonite block.

The temperature profiles of hole #6 show a sudden change in the inner part of the buffer in the interval starting at day 100 and ending at day 150. This could come from that the thermocouple TB612 at $r = 0.535$ comes into contact with the canister surface in this interval. More information on this topic can be found in /Hökmark et al., 2008/.

Using (3) once more and forming the ratio between the pellet slot conductivity and the bentonite block conductivity gives a possibility to study how the relation between the two conductivities evolves with time. Also, if an assumed conductivity of the bentonite block is multiplied with the obtained conductivity ratio an estimation of the pellet slot conductivity can be obtained. The assumed bentonite block conductivity is here taken as 1.2 W/(m·K), which is an estimate for the initial bentonite block conductivity based on the experimental findings in Figure 3-2. Thus, in this analysis the obtained pellet slot conductivity is underestimated when the bentonite becomes more saturated.

It should be noted that it is the effective conductivity of the materials that is considered. The heat transfer, especially in the pellet slot, is probably not only by conduction in reality, heat transfer by convection and radiation could also be present. The obtained pellet slot conduction should therefore be considered as an effective value.

In Figure 3-5 below the obtained conductivity ratio and estimated pellet slot conductivity are shown as a function of time since the corresponding heater was started (2003-05-08 for hole #5 and 2003-05-23 for hole #6).

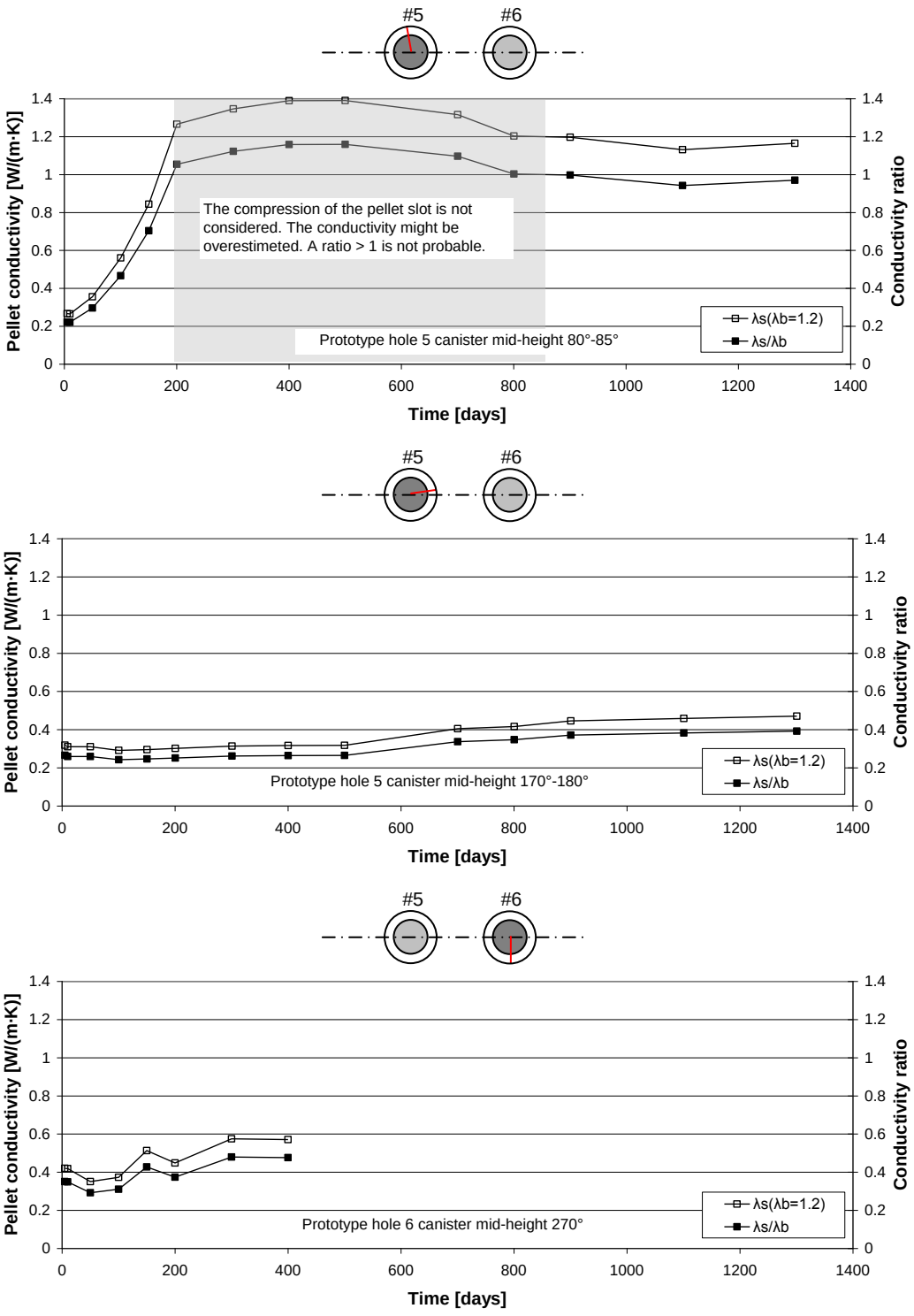

Figure 3-5 ***Conductivity ratio and estimated pellet slot conductivity at canister mid-height in hole #5 in the orientations 80°-85° (top) and 170°-180° (mid) and in hole #6 in the orientation 270° (bottom). Unrealistic results (ratio > 1) are indicated with a shaded area. Note that the time indicates number of days since the heater in the corresponding hole was started (2003-05-08 for hole #5 and 2003-05-23 for hole #6).***

For the 80°-85° direction in hole #5 the conductivity ratio > 1 between day 200 and day 850 which is unlikely. This indicates that the pellet slot width has decreased during the process and therefore the ratio is overestimated. The results after day 100 are not considered to be reliable in this direction.

In /Rhén and Forsmark, 2001/ mappings of the water bearing features in the boreholes can be studied. The map of hole #5 shows that there is a significant amount of water bearing features in the 80°-85° direction above and at canister mid-height. In the 170°-180° direction of hole #5 there are no water bearing features above or at canister mid height. The difference in the evolution of the pellet conductivity for different directions in hole #5 can therefore be explained by heterogenic water supply to the buffer.

For hole #6 in the 270° direction no water bearing feature is observed at canister mid-height, there is however one feature above canister mid-height (3.25 m from the tunnel floor) approximately in the 270° orientation.

Thus, a correlation between the obtained history of the pellet slot conductivity ratios and the position of the mapped water bearing features can be found.

Even though the conductivity ratio > 1 for the 80°/85° direction in hole #5, the initial results (at times less then 100 days) are however considered to be reliable for both directions. The obtained initial (at day 5) pellet slot conductivity of 0.27 W/(m·K) in the 80°-85° orientation and 0.32 W/(m·K) in the 170°-180° orientation of hole #5 is somewhat lower then expected. The average of the two values becomes 0.29 W/(m·K).

For hole #6 the initial (at day 5) pellet slot conductivity is 0.42 W/(m·K), but it decreases down to 0.35 W/(m·K) at day 50. The reason for the initial decrease in conductivity could come from that the pellet slot initially dries. When comparing the initial pellet slot conductivity between hole #5 and hole #6 is seems that hole #6 is at a more saturated state at the time when the heater was started. This is however in conflict with the inflow measurements that showed that hole #6 was more dry then hole #5.

The coinciding findings of hole #5, the unexpected higher conductivity of hole #6 and the doubtful drying process of hole #6 suggests that the result of hole #5 should be considered more accurate. The best estimate of the initial pellet slot conductivity is therefore considered to be 0.29 W/(m·K).

3.2.2 Water retention

Table 3-6 ***Retention constitutive law and adopted parameter values.***

Constitutive law	Parameter	Block	Pellets	Slot
Retention behavior, Van Genuchten $S_l = \left(1+\left(\frac{S}{p(T)}\right)^{1/(1-\lambda)}\right)^{-\lambda}$ $S = p_g - p_l$ $p(T) = p_0(n)\frac{\sigma(T)}{\sigma_0}$ $\sigma(T) = \left(1-0.625\frac{374.15-T}{647.3}\right)\left(0.2358\left(\frac{374.15-T}{647.3}\right)^{1.256}\right)$ $p_0(n) = p_0(n_0)e^{A(n_0-n)}$	p_0 [MPa]	30.130	1.124	0.5
	λ	0.152	0.271	0.6
	σ_0 [N/m]	0.072		
	n_0	0.355	0.602	-
	A	25.790	11.261	-

In the expression for the retention S_l is the water saturation, S the suction, p_g the gas pressure, p_l the liquid pressure, T the temperature and n the porosity. In the retention model the parameter value σ_0 = 0.072 N/m, for the surface tension, apply for all materials.

The point of departure when modeling the bentonite block retention behavior has been to consider laboratory data, data obtained from the model presented in /Dueck, 2005/ and to a smaller degree, as discussed in a former section, actual site data from the prototype experiment. Interest has only been taken to model the retention where $S_l > 0.85$, which is the range that is active in the simulated process.

The initial state of the bentonite has been taken as (S_l, S) = (0.864, 45 MPa). Using the initial state data, a set of points belonging to a suitable retention curve has been calculated using the model presented in /Dueck, 2005/. This set of points has been used to fit the parameters $p_0(n_0)$ and λ in the Van Genuchten retention model for $S_l > 0.85$. The obtained parameter values are $p_0(n_0)$ = 30.130 MPa and λ = 0.152.

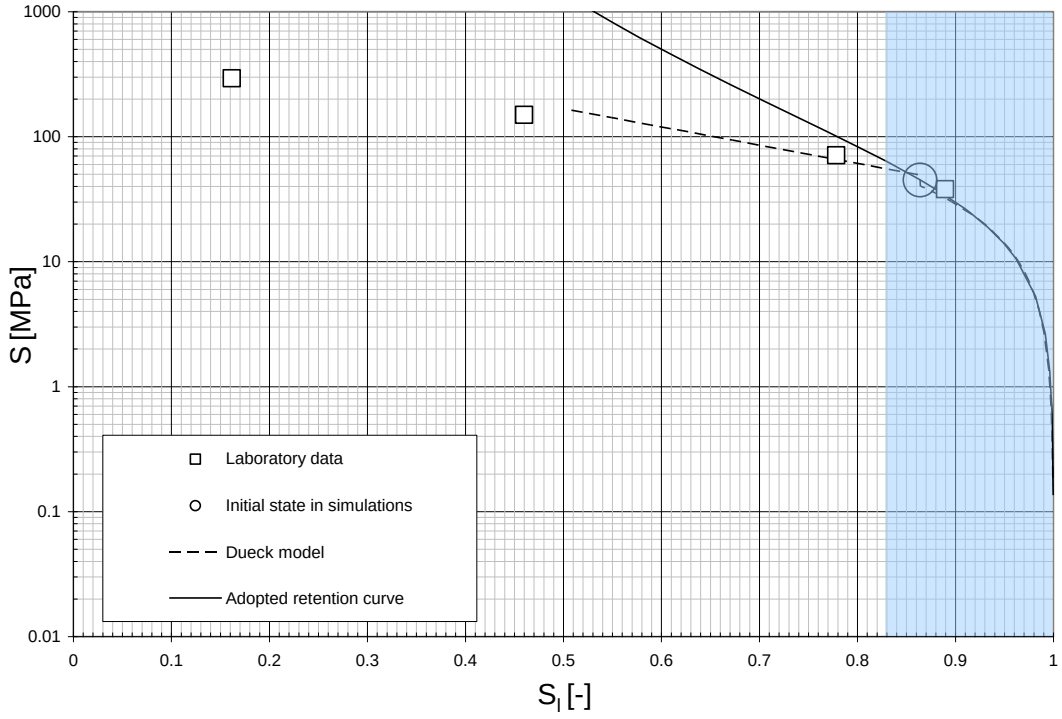

Figure 3-6 ***Bentonite block retention curve with the relevant water saturation range indicated with the shaded section.***

The porosity dependence has been incorporated by letting the parameter p_0 depend on porosity according to the boxed relation shown in Table 3-6. The parameter A in the relation was obtained by assuming that the mass of water, m_w, is constant during a porosity change from n_0 to n_1, where n_0 is the initial porosity and n_1 the approximate maximal porosity during the process. The outcome of the constant water mass assumption is the water saturation S_{r1} corresponding to n_1.

$$m_w = \rho_w S_{lo} e_0 V_p = \rho_w S_{l1} e_1 V_p \rightarrow S_{l1} \tag{4}$$

Now, by assuming a constant suction during the porosity change, $p_0(n_1)$ can be calculated.

$$S(S_{lo}, p_0(n_0)) = S(S_{l1}, p_0(n_1)) \rightarrow p_0(n_1) \tag{5}$$

The value of parameter A can now be obtained using the relation for $p_0(n)$.

$$p_0(n_1) = p_0(n_0) e^{A(n_0 - n_1)} \rightarrow A \tag{6}$$

The retention of the pellet slot has been obtained by scaling laboratory data with the void fraction (porosity) in the same fashion that was done when obtaining the parameter A for the bentonite block above and fit the parameters in the Van Genuchten model to this data. The obtained parameter values are $p_0(n_0)$ = 1.124 MPa and λ = 0.271. Also here a porosity dependency has been incorporated in the same way as for the bentonite block. The adopted retention curve is shown in Figure 3-7.

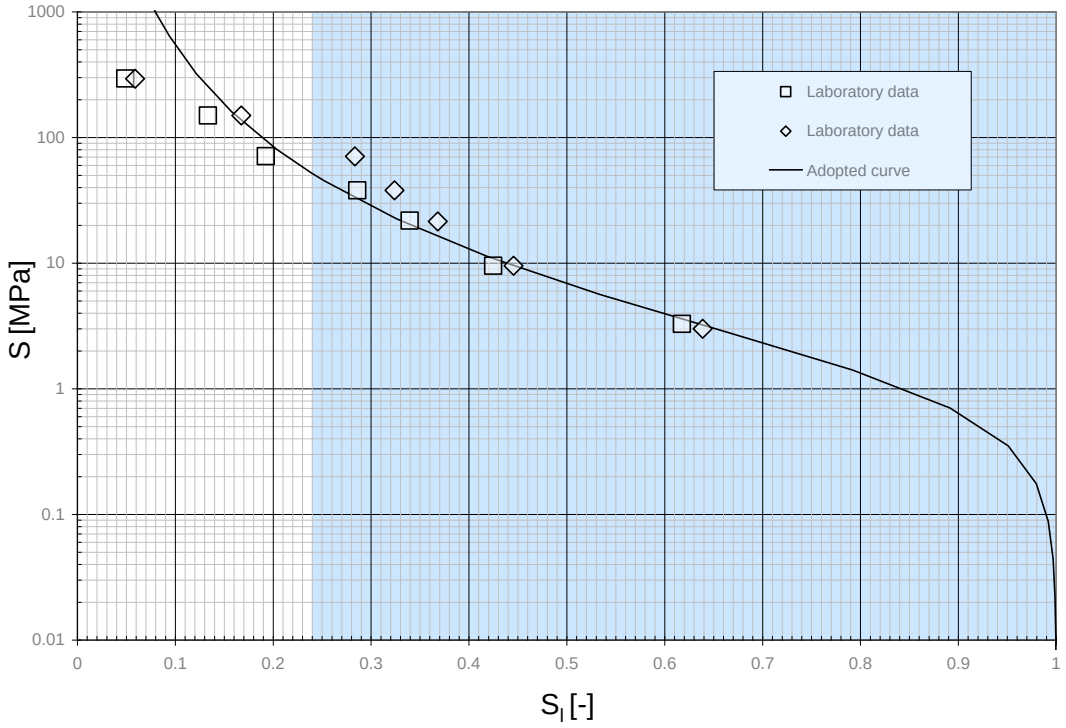

Figure 3-7 ***Pellet slot retention curve with the relevant water saturation range indicated with the shaded section.***

The inner slot retention parameters p_0 = 0.5 MPa and λ = 0.6 has been obtained from /Ledesma and Chen 2003/. No porosity dependency is adopted for the inner slot. The adopted inner slot retention curve is shown in Figure 3-8.

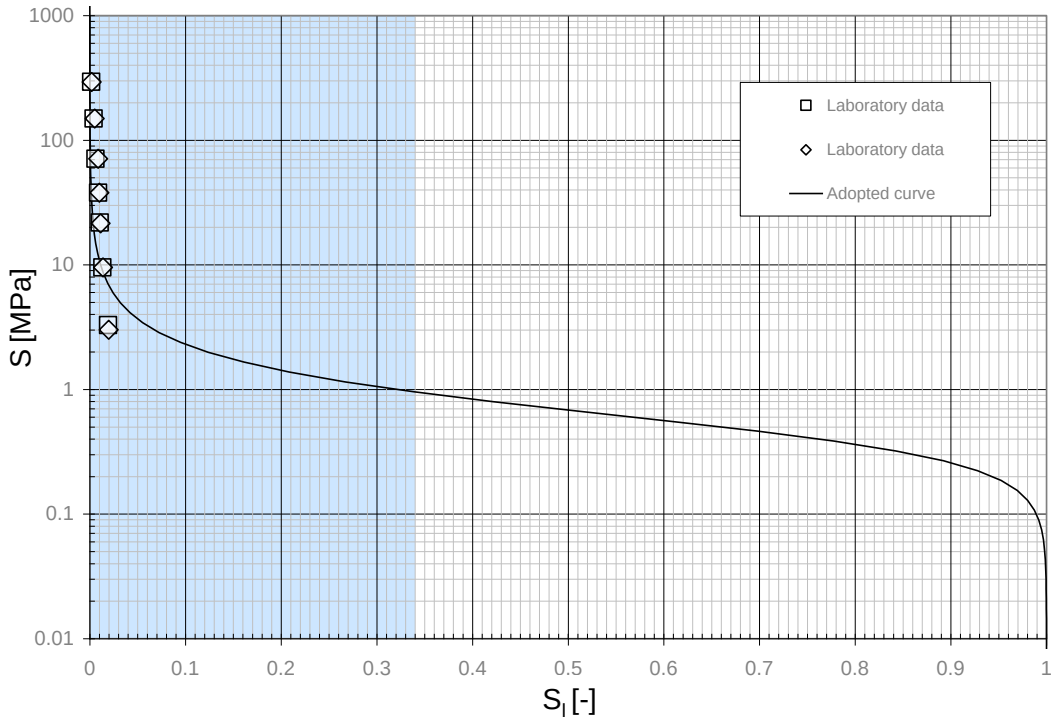

Figure 3-8 ***Inner slot retention curve with the relevant water saturation range indicated with the shaded section.***

3.2.3 Liquid water flow

Table 3-7 ***Constitutive model with parameter values for the flow through the porous medium.***

Constitutive law	Parameter	Block	Pellets	Slot
Flow through porous medium $\boldsymbol{q}_l = -\frac{k k_{rl}}{\mu_l}\nabla p_l$ $k = k_0 \frac{n^3}{(1-n)^2}\frac{(1-n_0)^2}{n_0^3}$ $k_{rl} = A S_l^{\lambda}$ $\mu_l = a\exp\left(\frac{b}{273.15+T}\right)$	k_0 [m^2]	$2\cdot10^{-21}$	$2\cdot10^{-19}$	$1\cdot10^{-11}$
	A	1		
	λ	3		
	n_0	0.355	0.602	0.98
	a [MPa·s]	$2\cdot10^{-12}$		
	b [K]	1808.5		

Above in the expression for the liquid flow through the porous medium $\boldsymbol{q}_l$ is the liquid flow, ∇p_l the gradient of the liquid pressure, n the porosity, S_l the liquid saturation and T the temperature. The same parameter values $a = 2\cdot10^{-12}$ MPa·s and $b = 1808.5$ K, present in the expression for the liquid viscosity, μ_l, have been used for all materials. The same expression of the relative permeability k_{rl}, where $A = 1$ and $\lambda = 3$, is also used for all materials.

The bentonite intrinsic permeability is set to $k_0 = 2 \cdot 10^{-21}$ at the reference porosity $n_0 = 0.335$, which equals the initial porosity. This agrees with the value shown in /Börgesson and Hernelind, 1999/.

The boxed equation in Table 3-7 shows that there is a possibility to let the relative permeability be dependent on the porosity in Code_Bright. There is not however any possibility for the user to influence this dependency, the relation is fixed. The question is therefore if the dependency should be incorporated or not in the model. In Figure 3-9 the hydraulic conductivity is plotted verses the void ratio for values found in /Börgesson and Hernelind, 1999/ and for the expression shown in Table 3-7.

As can be seen the expression underestimates the void ratio dependency to some extent.

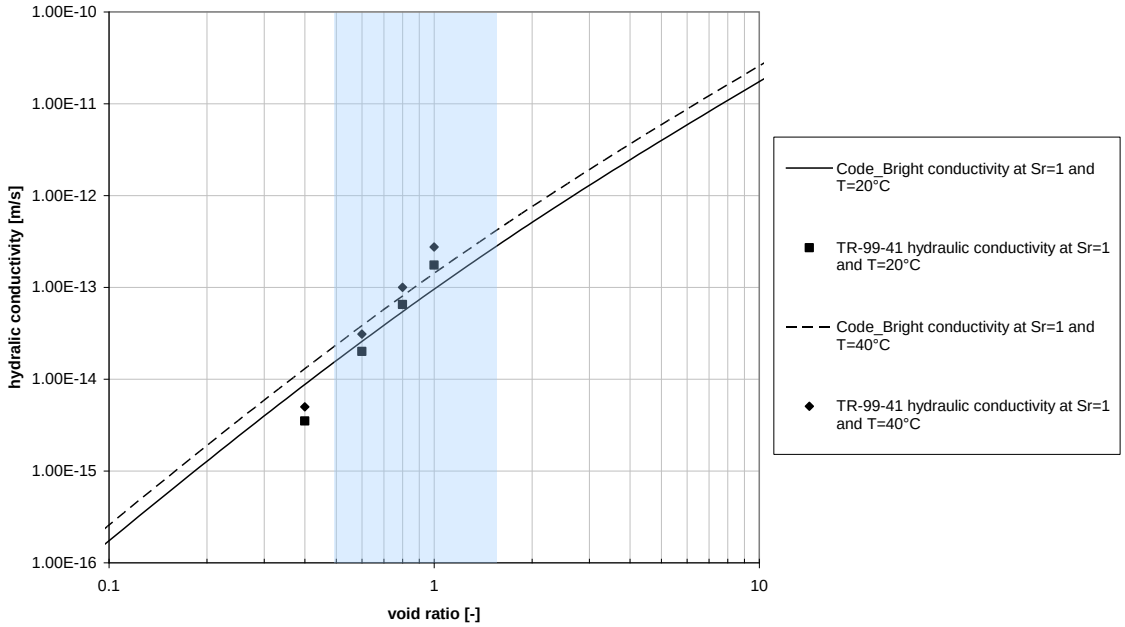

Figure 3-9 ***Hydraulic conductivity versus void ratio from /Börgesson and Hernelind, 1999/ and the expression used in Code_Bright. The relevant void ratio range is indicated with the shaded section.***

The pellets intrinsic permeability has been set to $k_0 = 2 \cdot 10^{-19}$ at the reference/initial porosity $n_0 = 0.602$, which has been obtained from /Börgesson and Hernelind, 1999/. This agrees with the findings in /Sugita et al 2003/ the permeability of the pellets is found to be approximately two magnitudes higher as compared to the bentonite block.

When it comes to the inner slot intrinsic permeability a value of $k_0 = 1 \cdot 10^{-11}$ has been adopted at the reference/initial porosity $n_0 = 0.98$.

3.2.4 Vapor diffusion

Table 3-8 ***Constitutive model and parameter values for the vapor diffusion.***

Constitutive law	Parameter	Block	Pellets	Slot
Vapor diffusion $\boldsymbol{i}_g^w = -(n\rho_g S_g D_m^w)\nabla\omega_g^w$ $S_g = 1 - S_l$ $D_m^w = \tau D \frac{(273.15+T)^a}{p_g}$	D [m^2·Pa/(s·K^n)]	$5.9\cdot10^{-6}$		
	A	2.3		
	τ	0.15	0.50	1.0

In the law of the water vapor diffusion, $\boldsymbol{i}^w{}_g$ is the vapor flux, n the porosity, ρ_g the gas density, S_g the gas saturation, $D^w{}_m$ molecular diffusion of vapor and $\nabla\,\omega^w{}_g$ the gradient of the mass fraction of water in gaseous phase. In the diffusion model D=5.9·10^{-6} m^2·Pa/(s·K^n) and a=2.3 have been used for all materials.

The tortuosity factor, τ, has been set to 0.15 for the bentonite block. This value is based on work presented by /Birgersson et al. 2007/. For the homogenized pellets slot, the factor is set to 0.5 and for inner slot to 1.0. The factor of tortuosity is not an easily determined quantity. In the Code_Bright vapor transport model it is a fixed constant /CIMNE, 2004/, whereas in reality it is likely to depend on saturation and temperature. For modeling of the high-temperature, high-thermal-gradient, mock-up test performed within the Temperature Buffer Test, the two modeling groups used very different values (0.3 and 1.0) for less saturated MX-80 bentonite of a density similar to that of the Prototype Repository bentonite blocks /Åkesson 2006/.

3.2.5 Mechanical behavior

The elastic part of Barcelona Basic Model (BBM, cf. /Alonso et al., 1990/) has been used to model the bentonite block and pellet slot. This model is formulated using the small strain assumption and accordingly the total strain increment $d\boldsymbol{\varepsilon}$ may be split into two incremental parts

$$d\boldsymbol{\varepsilon} = d\boldsymbol{\varepsilon}^m + d\boldsymbol{\varepsilon}^h \tag{7}$$

The two increments will in this work be referred to as the "mechanical strain increment" $d\boldsymbol{\varepsilon}^m$ and the "hydraulic strain increment" $d\boldsymbol{\varepsilon}^h$.

The strain can also be decomposed in a hydrostatic part $1/3\mathrm{tr}(\boldsymbol{\varepsilon})\boldsymbol{I} = -1/3\varepsilon_v\boldsymbol{I}$, where the volumetric strain $\varepsilon_v \approx -(dV - dV_0)/dV_0$ (dV and dV_0 denotes a material volume in the current and reference configuration respectively and the approximation is due to that higher order terms are neglected) is introduced, and a deviatoric part, $\boldsymbol{e} = \boldsymbol{\varepsilon} + 1/3\varepsilon_v\boldsymbol{I}$. Note that the definition of the volumetric strain gives that $\varepsilon_v > 0$ in compression. Thus, we obtain

$$\boldsymbol{\varepsilon} = -\frac{1}{3}\varepsilon_v{}^m\boldsymbol{I} + \boldsymbol{e}^m - \frac{1}{3}\varepsilon_v{}^h\boldsymbol{I} + \boldsymbol{e}^h, \tag{8}$$

where $\boldsymbol{e}^h = \boldsymbol{0}$ in the used material model.

The effective stress tensor $\boldsymbol{\sigma}'$ is defined by $\boldsymbol{\sigma}' = \boldsymbol{\sigma} + \max(p_l, p_g)\boldsymbol{I}$, where p_l denotes the liquid pressure and p_g denotes the gas pressure. The effective stress tensor are decomposed in a hydrostatic part $1/3\mathrm{tr}(\boldsymbol{\sigma}')\boldsymbol{I} = -p'\boldsymbol{I}$, where the effective pressure p' is introduced, and a deviatoric part $\boldsymbol{s} = \boldsymbol{\sigma}' + p'\boldsymbol{I}$.

Table 3-9 ***Constitutive model and parameter values for representing the mechanical behavior.***

Constitutive law	Parameter	Block	Pellets
"Mechanical strain increment" $d\boldsymbol{\varepsilon}^m = -1/3\ d\varepsilon_v^m \boldsymbol{I} + d\boldsymbol{e}^m$ $d\varepsilon_v^m = \frac{dp'}{K},\ K = \max\left\{\frac{(1+e)p'}{\kappa_i(s)}, K_{\min}\right\}$ $\kappa_i(s) = \kappa_{i0}(1+\alpha_i s)$ $d\boldsymbol{e}^m = d\boldsymbol{s}/2G,\ G = \frac{3(1-2\nu)}{2(1+\nu)}K$	κ_{i0}	0.25	2.5
	α_i	-0.017	0
	ν	0.2	0.2
	$K_{\min}$ [MPa]	10	5
"Hydraulic strain increment" $d\boldsymbol{\varepsilon}^h = -1/3\ d\varepsilon_v^h \boldsymbol{I}$ $d\varepsilon_v^h = \frac{\kappa_s(p',s)}{(1+e)(s+p_{atm})}ds$ $\kappa_s(p',s) = \kappa_{s0}\left(1+\alpha_{sp}\ln\frac{p'}{p_{ref}}\right)$	κ_{s0}	0.28	0.15
	α_{sp}	-0.16	0
	p_{ref}	0.1	0.1

The parameter values of the bentonite block have been prescribed according to what has been found when studying experimental findings.

The κ_{i0}-value was derived from results from a drained compression and swelling test presented by /Börgesson et al. 1988/. With an unloading from 900 kPa to 450 kPa, the void ratio increased from 0.90 to 1.07, which corresponds to a κ_i-value of approx. 0.25. The α_i-value is chosen so that κ_i is equal to zero for a suction level slightly higher than the highest occurring suction, so for a suction of 60 MPa this correspond to α_i = -0.017. In hindsight, it should be remarked that the chosen κ_{i0}-value is quite high, and that a lower value should have been adopted if relevant values for the plastic parameters (especially λ) would have been included.

A value for the Poisson's ratio were adopted from results from uniaxial compression test presented by /Kalbantner and Johannesson 2000/. These tests were performed on four unsaturated specimen with void ratios between 0.47 and 0.55 and water content of either 12 or 16 %. The measured values were 0.14, 0.17, 0.21 and 0.27, and a general value of 0.2 was therefore adopted.

The K_{min} value was set low ($\leq$ 20 MPa) in order to adhere to the BBM as far as possible.

The κ_{s0}-value was derived from results from swelling tests with constant zero axial load /Dueck 2004/. A series of tests with the same initial void ratio water content were exposed to different relative humidity climates, after which the void ratio were determined. The steps between two such final void ratios were evaluated. Swelling for suction values from 40 to 3 MPa, and void ratios from 1.27 to 1.96 corresponds to a κ_s-value of 0.27. For swelling from 25 to 3 MPa, and 1.35 to 1.96, respectively, the corresponding modulus was 0.29. Hence, a general κ_{s0}-value of 0.28 was adopted. Since no suction dependence of the modulus could be found, the α_{ss}-value was set to zero.

Finally, the α_{sp}-value can be set to correspond to the swelling pressure of the block density. The swelling pressure for the block density is approx. 40 MPa ($2 \cdot 0.57^{(-1/0.187)}$, see /Börgesson et al. 1995/), and together with a p_{ref}-value of 0.1 MPa, this corresponds to a α_{sp}-value of -0.17. A slightly lower value (-0.16) was adopted in an attempt to mimic the swelling pressure curve.

In the pellet slot, the parameters have been calibrated so that the void ratio profile at full saturation agrees with measurements in the Canister Retrieval Test /Johannesson, 2007/ and that the stress buildup is comparable with the measured stress in hole #1. As Table 3-9 shows, a quite plain pellet slot mechanical representation has been used, where α_i=0 and α_{sp}=0. This simplifies the calibration procedure where the void ratio profile at full saturation, here taken as the void profile after 6000 days, is fitted against the CRT data and the stress is fitted against experimental measurement in hole #1 by adjusting the values of κ_{i0} and κ_{s0}.

This representation of the mechanical behavior of the materials, where only the elastic part of BBM is active, is relatively simple. The used model is not considered to provide an accurate representation of the mechanical behavior of compacted bentonite subjected to a wide range of THM processes or at different densities. For the present purposes however, where mainly the degree of influence from the mechanical process is studied and the question whether the mechanical homogenization (the interaction between the block and the pellet slot) can be captured or not is investigated, the model is believed to be sufficient. In this perspective it seems suitable to use this simple model which later on can be "upgraded" using the plasticity or replaced with other more representative models.

The inner slot is modeled mechanically using linear elasticity. At first the slot material is prescribed as weak so that the slot can be closed. When the slot dimension is small enough the slot is prescribed as stiff so that no further slot deformation takes place. This hands on procedure is used since Code_Bright presently lack contact elements.

3.3 Boundary conditions

To complete the model description thermal, hydraulic and mechanical boundary conditions have to be specified. In Figure 3-10 a schematic graphical overview is given of the boundary conditions prescribed in the model.

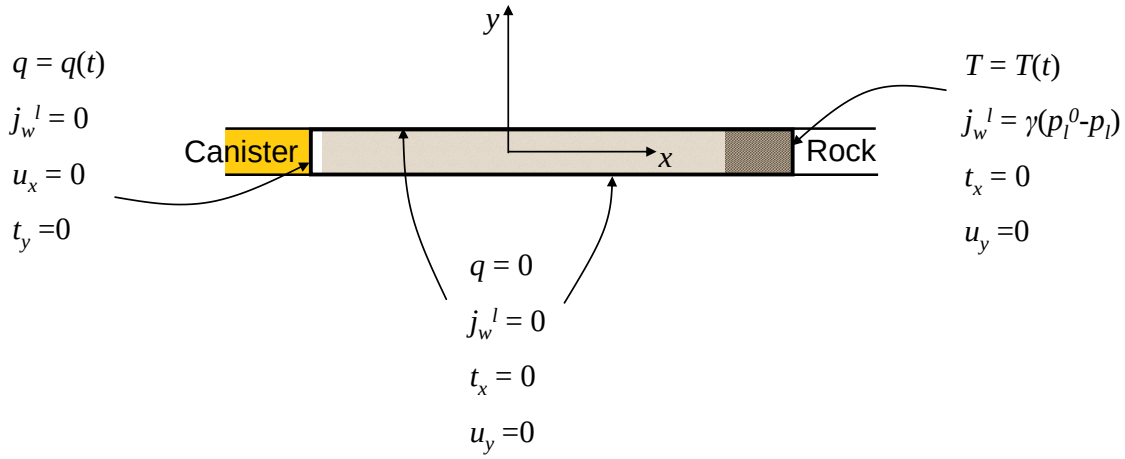

Figure 3-10 ***Schematic geometry with the prescribed boundary conditions.***

In the following list the variables defining the boundary conditions are declared.

- Thermally: q is the heat flux, T is the temperature
- Hydraulic: j_w^l is the liquid water flux, p_l the liquid pressure, γ the leakage coefficient

- Mechanically: u_i is the displacement in the i-direction, where $i = x$ or y, and t_i is the traction component in the i-direction. If unit vectors $\boldsymbol{e}_n$ and $\boldsymbol{e}_t$ are introduced, denoting unit vectors in the normal and tangential direction of the boundary surface respectively, the boundary conditions can be expressed $\boldsymbol{e}_n \cdot \boldsymbol{u} = 0$ and $\boldsymbol{e}_t \cdot \boldsymbol{t} = 0$.

3.3.1 Thermal boundary conditions

The thermal boundary conditions of the 1D model are obtained from a large 3D thermal model, where the whole experimental site, including tunnel, holes, backfill, concrete plugs, buffer and canisters are included. Here the thermal boundary conditions, the heat flux at the canister surface and the temperature at the rock wall, taken from the 3D model are shown in Figure 3-12. For more information about the 3D model and how the boundary conditions were extracted from the model, see /Kristensson and Hökmark, 2007/. Figure 3-11 shows the measured and simulated temperature evolution in the rock close to deposition hole #1 and deposition hole #3.

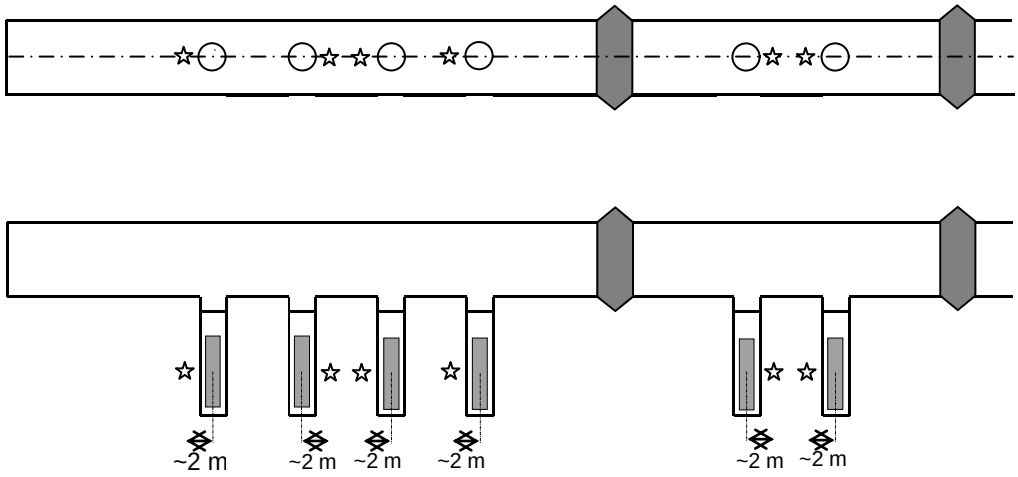

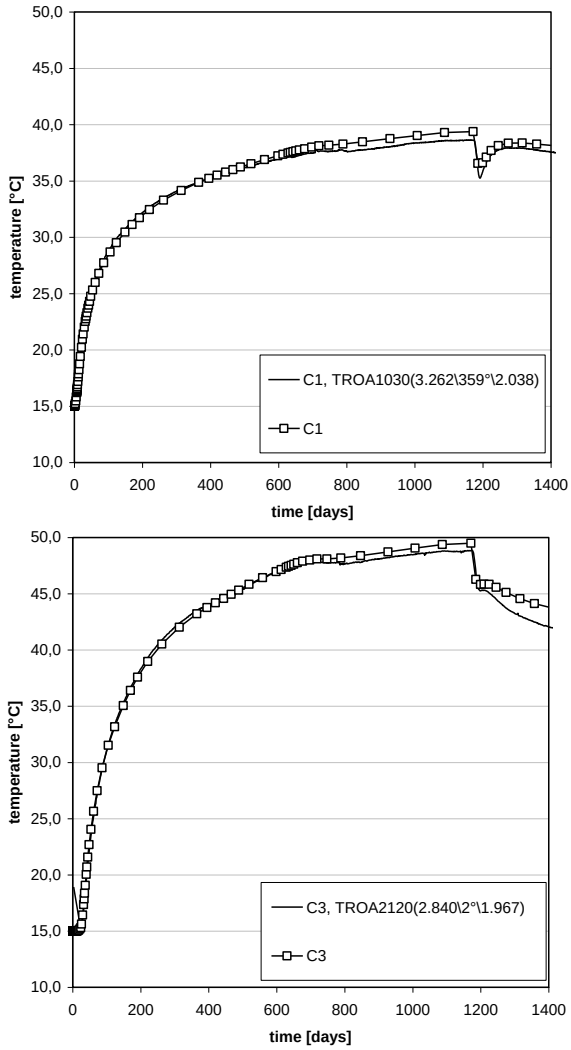

Figure 3-11. ***Upper: Horizontal and vertical sections of Prototype Repository where the thermocouple-positions in the rock are indicated. Lower: Measured and simulated temperature evolutions close to hole #1 (left) and hole #3 (right)***

In the 3D model, asymmetric effects in the heat flux field and the temperature field due to heat contribution from neighboring canisters are accounted for. The extracted boundary conditions from the 3D model, used in the local buffer model in this work, can therefore be specified for any specific point at the canister.

In the local model though, the assumed radial symmetry makes the model only suitable where the processes are very close to radial, i.e. at the mid-height of the canister, and the prescribed boundary conditions will due to the rotational symmetry also be constant around the inner and outer boundaries.

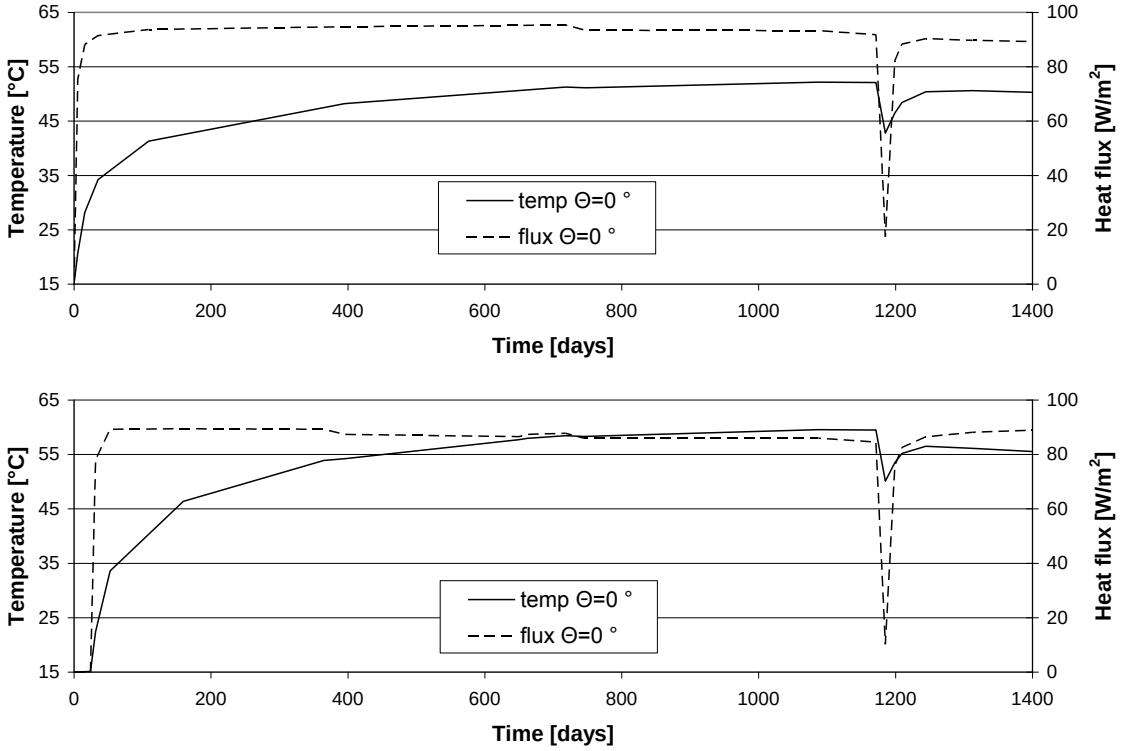

Figure 3-12 ***Thermal boundary conditions for deposition hole #1 (top) and deposition hole #3 (bottom).***

In /Kristensson and Hökmark, 2007/ the simulated heat flux at canister mid-height obtained from the thermal 3-D model at day 395 (day 0 is defined as 2001-09-17 which was the date when the heaters in canister #1 were started) was evaluated in hole #1 and hole #3. The evaluation was performed by calculating the bentonite block conductivity inserting the simulated heat flux, measured bentonite block temperatures and the sensor radial positions in equation (3). Below follows an updated version of this evaluation for hole #1 and hole #3 with more estimates of bentonite conductivities and where the sensors used are identified for clarity.

For each hole there are three tables giving the information used in the investigation. In the first set of tables, Table 3-10 and Table 3-11, the positions where the bentonite conductivity is estimated are defined (also shown schematically in Figure 3-13), the sensors used are identified and the measured temperatures at day 395 are shown. The second set of tables, Table 3-12 and Table 3-13, contains the simulated radial heat flux in different orientations at day 395, and the third set of tables, Table 3-14 and Table 3-15, shows the obtained bentonite block conductivity for the different locations at day 395.

Table 3-10 ***Position identification where the sensors used and measured temperatures for hole #1 are shown for day 395.***

ID	Orientation [°]	Radial position [mm]	Sensor label and position (z\α\r)	Measured temperature [°C]
A1	0	at r_1 = 635	TBU10011 (2980\0°\635)	65.43
		at r_2 = 735	TBU10012 (2980\0°\735)	59.57
B1	350	at r_1 = 585	WBU10013 (2870\350°\585)	69.14

		at r_2 = 685	WBU10014 (2870\350°\685)	62.73
C1	270	at r_1 = 585	TBU10019 (2980\270°\585)	69.02
		at r_2 = 635	TBU10020 (2980\270°\635)	66.21
D1	175	at r_1 = 585	TBU10016 (2980\175°\585)	69.48
		at r_2 = 685	TBU10017 (2980\175°\685)	63.73

Table 3-11 ***Position identification where the sensors used and measured temperatures for hole #3 are shown for day 395.***

ID	Orientation [°]	Radial position [mm]	Sensor label and position (z\α\r)	Measured temperature [°C]
A3	350	at r_1 = 585	WBU30013 (2840\350°\585)	74.63
		at r_2 = 685	WBU30014 (2840\350°\685)	69.52
B3	0	at r_1 = 635	TBU30011 (2971\0°\635)	71.42
		at r_2 = 735	TBU30012 (2971\0°\735)	67.13
C3	90	at r_1 = 585	TBU30013 (2971\90°\585)	71.53
		at r_2 = 685	TBU30014 (2971\90°\685)	67.09
D3	90	at r_1 = 685	TBU30014 (2971\90°\685)	67.09
		at r_2 = 785	TBU30015 (2971\90°\785)	61.77
E3	90	at r_1 = 585	TBU30013 (2971\90°\585)	71.53
		at r_2 = 785	TBU30015 (2971\90°\785)	61.77
F3	270	at r_1 = 585	TBU30019 (2971\270°\585)	77.46
		at r_2 = 635	TBU30020 (2971\270°\635)	74.20
G3	270	at r_1 = 635	TBU30020 (2971\270°\635)	74.20
		at r_2 = 685	TBU30021 (2971\270°\685)	71.58
H3	270	at r_1 = 585	TBU30019 (2971\270°\585)	77.46
		at r_2 = 685	TBU30021 (2971\270°\685)	71.58

Table 3-12 ***Simulated heat flux for hole #1 at day 395.***

Orientation [°]	Simulated heat flux [W/m^2]
0	94.73
90/270	91.36
180	81.93

Table 3-13 ***Simulated heat flux for hole #3 at day 395.***

Orientation [°]	Simulated heat flux [W/m^2]
0	87.35
90/270	91.06

Table 3-14 ***Obtained estimations of the bentonite conductivity for hole #1 at day 395.***

ID	A1	B1	C1	D1
Conductivity [W/(m·K)]	1.24	1.22	1.40	1.18

Table 3-15 ***Obtained estimations of the bentonite conductivity for hole #3 at day 395.***

ID	A3	B3	C3	D3	E3	F3	G3	H3
Conductivity [W/(m·K)]	1.42	1.56	1.70	1.22	1.44	1.20	1.38	1.28

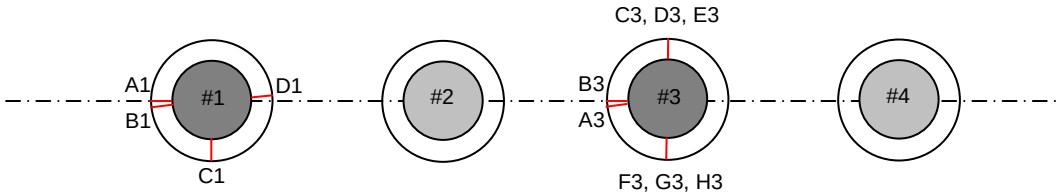

Figure 3-13 ***Schematic drawing of the inner section (hole #1 - hole #4), where the positions for which estimates of the bentonite conductivity is calculated.***

Taking the average of all conductivities in hole #1 gives a value of 1.26 W/(m·K) and taking the average of all conductivities in hole #3, neglecting the unphysical value of 1.7 W/(m·K), gives a value of 1.36 W/(m·K).

The results are in contrast to the lab-scale results shown in Figure 3-2: The dry hole thermal conductivity is higher than the saturated lab-scale conductivity and the wet hole conductivity is lower. The differences are, however, not great and can largely be attributed to the different ways the surface heat flux is distributed over the canister surface area:

- In the dry hole, there is an insulating vertical air gap that tends to direct some of the heat output towards the base/top regions, where there is direct thermal canister-bentonite

contact. The mid-height heat flux is correspondingly reduced, giving a high apparent conductivity at mid-height..

- In the wet hole, the base/top regions are those likely to be least saturated, possibly with some heat flow direction towards the mid-height regions. This will tend to reduce the apparent thermal conductivity at mid-height.

Here the thermal boundary flux was set without consideration of any saturation-induced disturbances of the heat flow distribution.

3.3.2 Hydraulic boundary conditions

The hydraulic conditions are prescribed as impermeable at all boundaries except for the interface between the pellets slot and the rock wall. At the rock wall different water inflow conditions are modeled for the different holes by prescribing different leakage coefficients γ. This approach has been adopted since it is not easy to model the pressure evolution in the Prototype Repository rock mass directly at the hole wall. The available amount of data is small and the pressures are measured in sealed boreholes over a long distance which gives poor precision in position.

The boundary water pressure is also not considered to governing the saturation process, since the suction in the buffer is much larger. The access of water at the rock wall, i.e. the water flux, is considered to be of more importance for the saturation evolution. Thus, in the simulation, the prescribed constant boundary water pressure p_l^0 together with the used leakage coefficient is governing the saturation process in the simulation, since the boundary water flux j^w_l is given by,

$$j^w_l = \gamma \, (p_l^0 - p_l) \tag{9}$$

, where p_l is the current water pressure at the boundary and j^w_l is defined as positive for injection into the medium. The water pressure is here prescribed equal to the adopted gas pressure, i.e. $p_l^0 = 0.1$ MPa.

Experimental measurements of the pressure head in the rock mass: KA3584G01:2 (between hole #1 and hole #2), KA3578G01:2 (between hole #2 and hole #3), KA3576G01:(2,3) and KA3574G01(1,2,3) (close to hole #3) see /Goudarzi and Johannesson, 2007/, all show that the water pressure in the rock mass close to the deposition holes is below 0.2 MPa, except for when the pressure peaked just before the drainage was opened. The used constant value of the boundary water pressure, 0.1 MPa, therefore seems applicable close to hole #1 and hole #3.

To obtain a representative water flux the value of the leakage coefficient γ is calibrated comparing simulated suction curves against measured suction curves at corresponding radial distances. Most emphasis is made fitting the suction curve close to the rock wall where the transport properties of the buffer materials are less influential.

In this way, the different hydraulic conditions of the different holes are modeled by prescribing different values of leakage coefficient. The used values of leakage coefficient adopted for hole #1 and hole #3 are shown in Table 3-16.

Table 3-16 ***Leakage coefficient values***

Hole no.	γ [kg/(s·MPa)]
1	$5 \cdot 10^{-7}$
3	$5 \cdot 10^{-11}$

3.3.3 Mechanical boundary conditions

The entire outer boundary is equipped with roller boundaries, i.e. no normal displacement, $\boldsymbol{e}_n \cdot \boldsymbol{u} = 0$, and no tangential traction, $\boldsymbol{e}_t \cdot \boldsymbol{t} = 0$, are allowed at the boundary surfaces.

3.4 Model overview

The models used in this work are categorized in Table 3-17 and Table 3-18 for hole #1 and hole #3 respectively. As presented above, the only difference between the models for the different holes are the boundary conditions. In the overview, the number of elements, the presence of mechanics, presence of porosity dependent permeability $k(n)$, see Table 3-7, presence of porosity dependent suction $S(n)$, see Table 3-6, and the used value of toruosity, τ, are indicated.

Table 3-17 ***Overview where the models used for hole #1 are characterized.***

Model name	Elements	Mechanics	$k(n)$	$S(n)$	τ
Base Case or THM1, $k(n)$, $S(n)$	1×103	X	X	X	0.15
Coarse	1×35	X	X	X	0.15
Fine	1×204	X	X	X	0.15
THM1, $k(n)$	1×103	X	X		0.15
THM1	1×103	X			0.15
TH1	1×103				0.15
THM1 (τ = 1.0)	1×103	X			1.0

Table 3-18 ***Overview where the models used for hole #3 are characterized.***

Model name	Elements	Mechanics	$k(n)$	$S(n)$
THM3, $k(n)$, $S(n)$	1×103	X	X	X
TH3	1×103			

4 Results and discussion

In this section results in form of temperature-, suction-, stress-histories at three radial distances, r = 0.585 m, r = 0.685 m and r = 0.785 m, are shown for hole #1 and hole #3. The obtained void ratio profiles at full water saturation are also shown for hole #1. In Figure 4-1 a schematic picture indicates the sensor locations at canister mid height, corresponding to the radial distances presented above, that are used to compare the simulation results with.

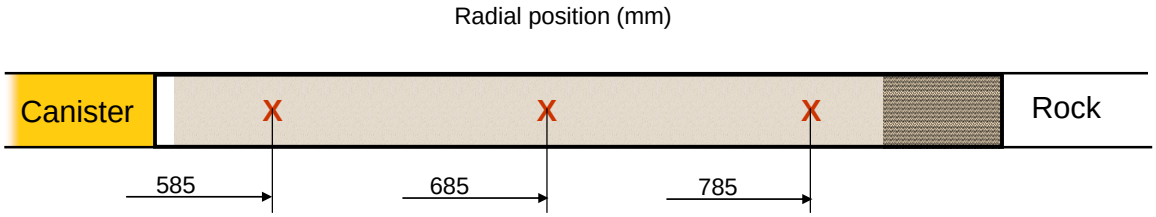

Figure 4-1 ***Sensor positions in which the simulations are compared with the experimental data.***

First a mesh dependency investigation is performed for hole #1. The simulation of hole #1 has been used for calibrating the material parameters and investigating the porosity/mechanical dependence on the thermal and hydraulic process. The simulation of hole #3 has been used for verification of the model generality (i.e. confirming that the modeling philosophy holds).

4.1 Mesh dependence

A mesh dependency investigation is performed for the problem where hole #1 is modeled. The convergence of the solutions obtained with different mesh densities is indicating if the mesh density is high enough. In Table 4-1 the used models are listed.

Table 4-1 ***Model overview where the models used in the mesh dependency investigation are characterized.***

Model name	Elements	Mechanics	$k(n)$	$S(n)$
Base Case	1×103	X	X	X
Coarse	1×35	X	X	X
Fine	1×204	X	X	X

Three meshes; the *Coarse* mesh 1×35, the *Base Case* mesh consisting of 1×103 elements and the *Fine* mesh of 1×204 elements, are used in the investigation. The quadrilateral elements used have linear shape functions and 4 integration points. A selective integration by means of the modification of the **B** matrix is used for the elements.

The solutions obtained with the Coarse and Base Case meshes are compared with the solution of the Fine mesh by forming the "relative difference" in some variables, i.e. relative difference = [variable(Coarse or Base Case) – variable(Fine)]/variable(Fine). Studying the relative differences in the variables the convergence of the solution with respect to the number of elements indicates whether the mesh density is high enough.

The variables investigated are: temperature evolution at radial distances 0.585 m, 0.685 m and 0.785 m, suction evolution at radial distances 0.585 m, 0.685 m and 0.785 m, the axial stress evolution at the radial distance 0.685 m, and the void ratio profile at full water saturation. The

first three variables, temperature, suction and axial stress are evaluated for day 25, 50, 100, 200, 400, and 800, and the void ratio profile is evaluated for day 6000. The result is shown in Figure 4-2.

The temperatures show a very low magnitude of relative difference between the different mesh alternatives. Thus, there is no significant mesh dependency for the temperature in the Base Case and the Coarse mesh.

For the suction the mesh dependency is clearly visible for the Coarse mesh especially early in the process. The Base Case also shows some mesh dependency, which a relative difference of < 2.5 % indicates, during the first 100 days in the simulation. In the remaining part of the simulation the relative difference drops down to maximum 1.5 % . The obtained indication of mesh dependency in suction of the Base Case is considered to be acceptable.

The axial stress responses show the same indication of mesh dependency as the suction responses above. The mesh dependency for the Base Case, indicated by < 1 % relative difference, is therefore considered insignificant with respect to the axial stress response.

Finally, the void ratio profile of the Base Case also indicates, with a relative difference < 1 %, that there is not a significant mesh dependency with respect to this variable either.

In conclusion, the Base Case mesh is found to discretize the problem to a degree that is sufficient.

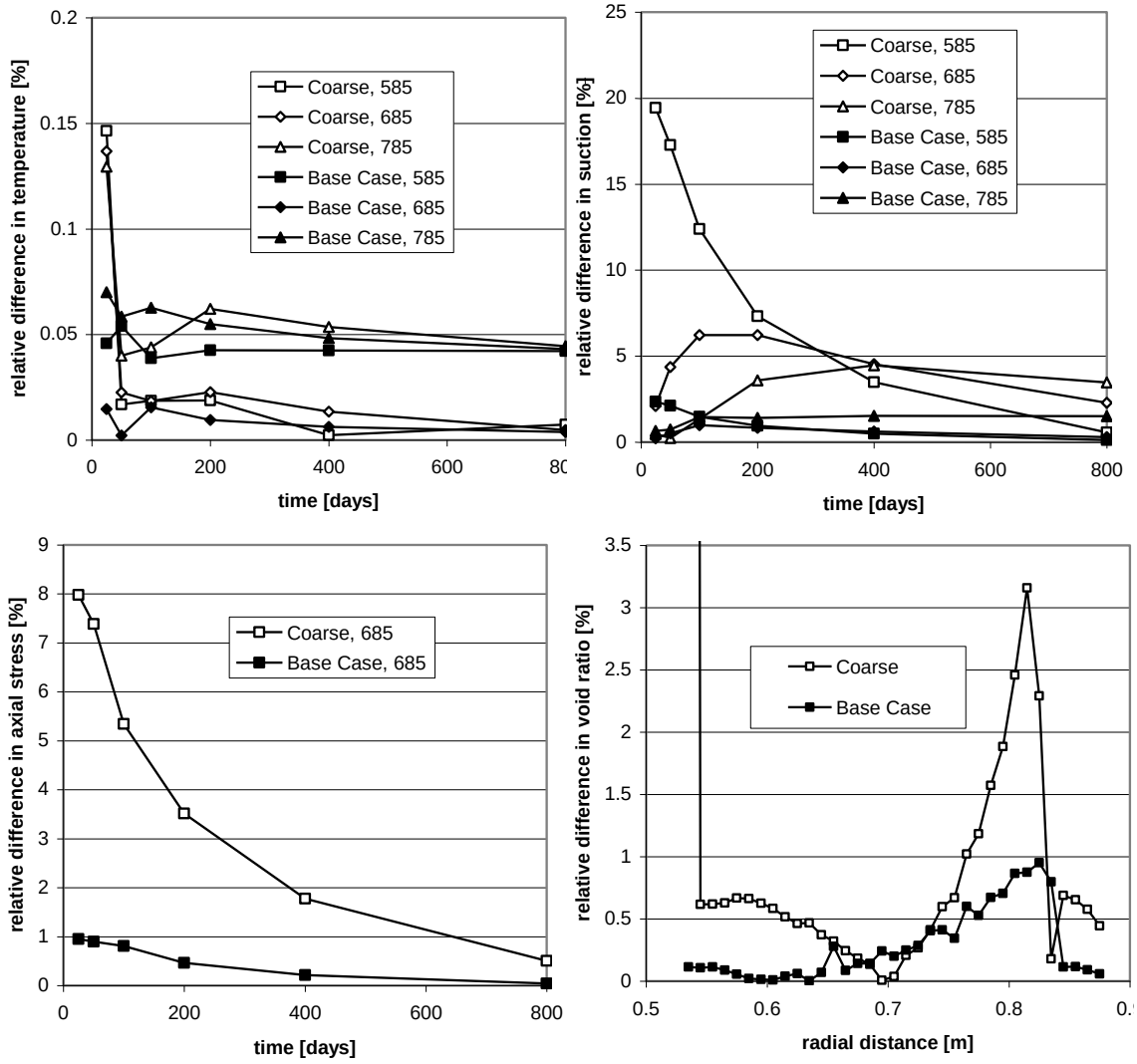

Figure 4-2 ***Relative differences, [var(Coarse) – var(Fine)]/var(Fine) and [var(Base Case) – var(Fine)]/var(Fine). The results are shown for the variables: temperature, suction, axial stress and the void ratio profile.***

4.2 Hole #1 (wet conditions)

For hole #1 the different porosity dependencies as well as the dependency from the mechanical process are investigated. Table 4-2 shows the used models and Table 4-3 identifies the sensors used when performing comparisons between experiments and simulations. Day 0 is defined at 2001-09-17 which was the date when the heaters in canister #1 was started.

Table 4-2 ***Model overview where the models used in the simulation of hole #1 are characterized.***

Model name	Elements	Mechanics	$k(n)$	$S(n)$	τ
THM1, $k(n)$, $S(n)$	1×103	X	X	X	0.15
THM1, $k(n)$	1×103	X	X		0.15
THM1	1×103	X			0.15
TH1	1×103				0.15
THM1 (τ = 1.0)	1×103	X			1.0

Table 4-3 ***Sensor label, position and measured variables for the sensors used for the comparisons made in hole #1.***

Sensor label	WBU10013	WBU10014	WBU10015	PBU10011
Sensor position ($z\backslash\alpha\backslash r$)	(2.870\350°\0.585)	(2.870\350°\0.685)	(2.870\350°\0.785)	(2.780\5°\0.685)
Measured variable	*RH, T*	*RH, T*	*RH, T*	σ_a

4.2.1 Thermal response

Temperature

In Figure 4-3 - Figure 4-5 the measured and simulated temperature histories are shown for the different radial positions. The simulated temperatures underestimate the experimental temperatures in the first part of the experiment. It can be seen that the porosity and the mechanics do not significantly affect the temperature.

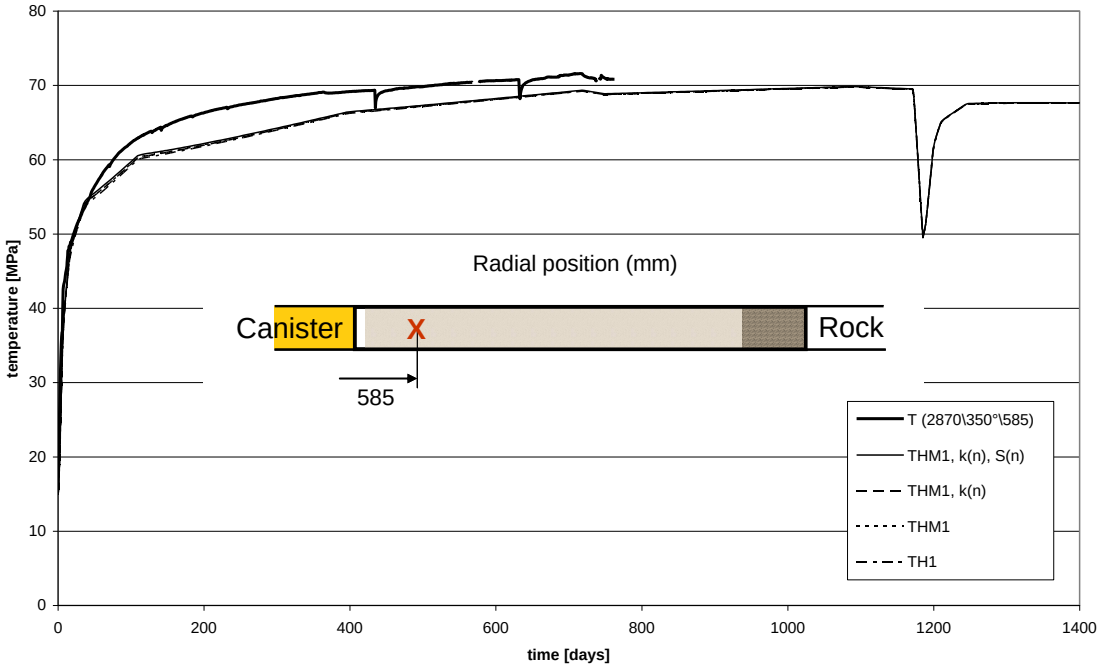

Figure 4-3 ***Experimental, WBU10013(2.870\350°\0.585), and simulated temperatures at r=0.585 m for hole #1.***

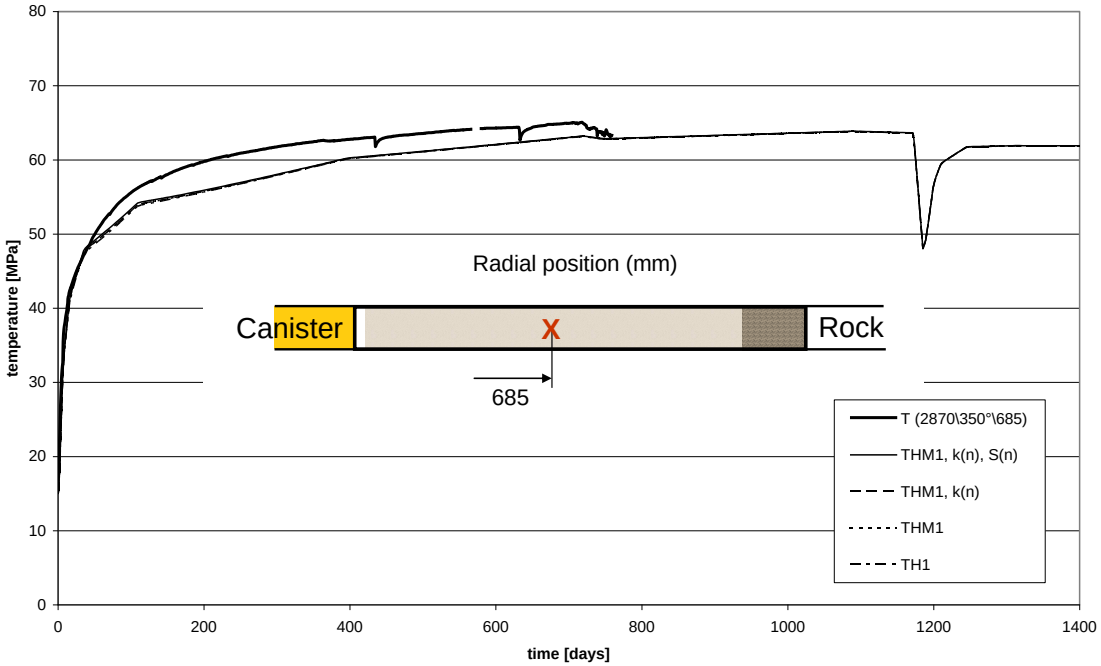

Figure 4-4 ***Experimental, WBU10014(2.870\350°\0.685), and simulated temperatures at r=0.685 m for hole #1.***

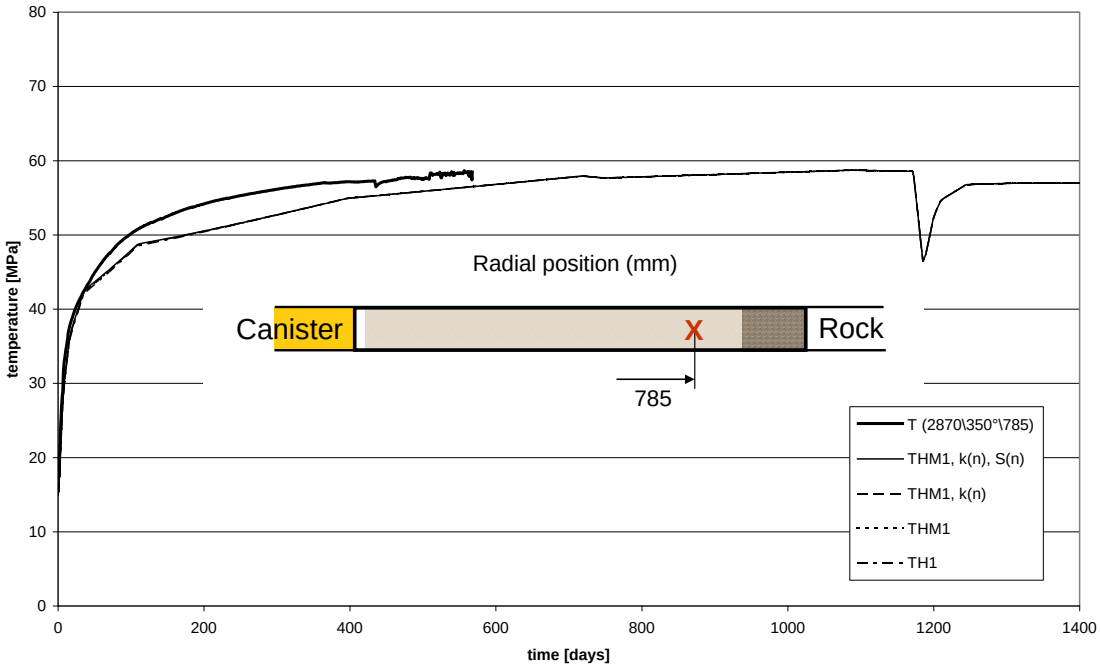

Figure 4-5 ***Experimental, WBU10015(2.870\350°\0.785), and simulated temperatures at r=0.785 m for hole #1.***

In Figure 4-6 the temperature profiles in the buffer in the experiment and of THM1, *k*(*n*), *S*(*n*) (the Base Case) are shown after 10, 100 and 400 days.

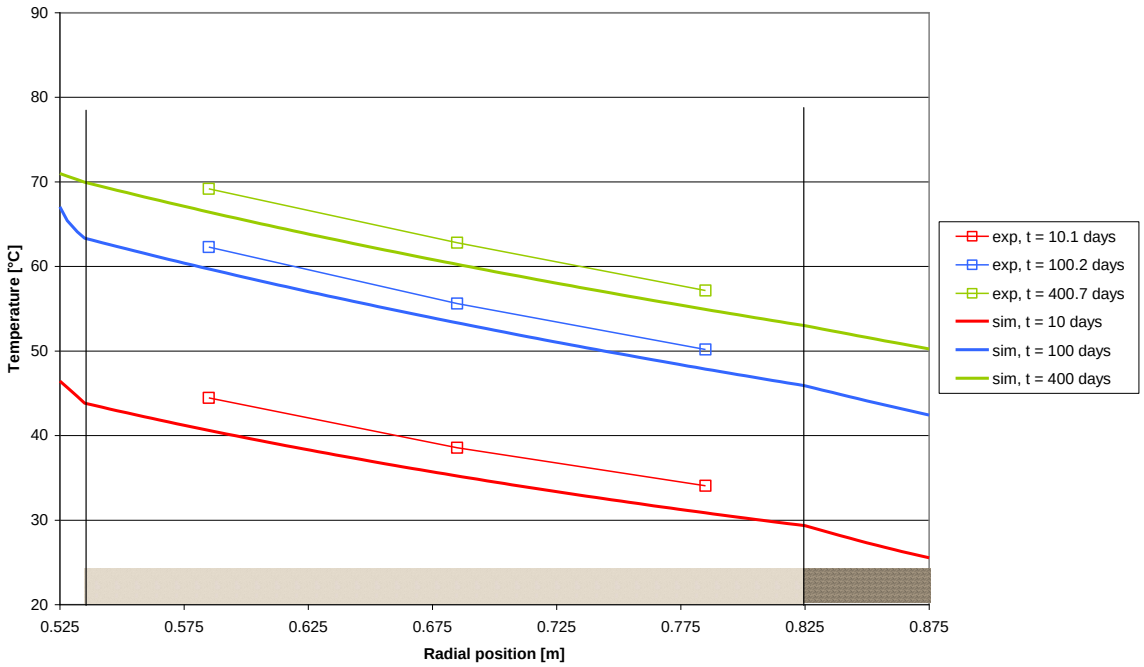

Figure 4-6 ***Experimental and simulated temperature profiles in the buffer after 10, 100 and 400 days (hole #1 simulation).***

The temperature gradient in the block is captured correctly in the simulation. A qualitative comparison with the experimental results for hole 5, see Figure 3-4, shows that the model produces results that resembles the experiment with a temperature gradient in the pellet slot that decreases with time. The temperature profiles also show that the simulated temperatures are lower then the experimental temperatures in the block.

The exact reason for the discrepancy is difficult to pinpoint. There discrepancy could of course arise from combinations of several defects in the model. Some possibilities could however be suggested:

1. The rock temperature is too low.
2. A combination of too low canister heat flux and too low block conductivity.
3. The pellet slot conductivity is too high.
4. The radial assumption is not valid due to non-radial contributions.

A brief discussion of the possibilities listed above is given in the following.

1. The rock temperature is too low.
The rock temperature is obtained from the thermal 3D analysis. In /Kristensson and Hökmark, 2007/, where the 3D simulation is described, it was found that the model produced slightly lower temperatures, approximately 1 °C, close to the hole walls of hole #5 and hole #6. The temperatures 2 m from the hole centers (in the pillars between the holes) were however well reproduced.

This could be a consequence of that the temperature in the pillars are governed by the average conductivity in a larger volume as compared to the temperatures close to the hole walls. The hole wall temperature is therefore more sensitive to local thermal conductivity variations

which could explain why experimental and simulated temperatures coincide in the interior of the pillars, but not equally well in the rock wall..

2. A combination of too low canister heat flux and too low block conductivity.
When studying the experimental data in Figure 3-2 and also the findings in /Kristensson and Hökmark, 2007/ (this investigation is also repeated in this report in an updated version in section 3.3.1), where the bentonite block conductivity were evaluated using the measured temperatures and the radial heat flux of the thermal 3D model, an initial bentonite block conductivity of 1.164 W/(m·K), as used in the present model, seems lower than necessary. This value could be increased up to approximately 1.2 W/(m·K) to match the experimental results shown in Figure 3-2 and the findings in section 3.3.1.

To obtain the same temperature difference in the bentonite block with the new bentonite block conductivity the flux has to be increased with the ratio 1.2 / 1.164 = 1.031, i.e. in increase of 3.1 %.

The radial heat flux used in the 1D radial models is obtained from the thermal 3D analysis. In the 3D model the buffer has been allotted homogeneous thermal properties. If there are inhomogeneous thermal properties in the experiment, the radial heat flux could therefore differ from the simulated one since more or less heat flux may escape at different locations due to the heterogeneity. Heterogeneous wetting of the buffer would give a heterogeneous conductivity distribution.

3. The pellet slot conductivity is too high.
In the investigation of the pellet slot conductivity, see section 0, an initial pellet slot conductivity of 0.29 W/(m·K) was obtained. The used model gives an initial pellet slot conductivity of 0.42 W/(m·K) which indicates that the parameters in the model could be adjusted in order to lower the pellet slot conductivity.

4. The radial assumption is not valid due to presence of non-radial contributions.
As discussed above, heterogeneous thermal properties may be present in the experiment and as a consequence the processes may be non-radial at the canister mid-height, i.e. there will be axial and/or tangential flow of heat flux that cannot be represented with the used radial assumption.

Heat flux

To study the heat transfer in the simulation, profiles of the conductive heat flux are shown for day 10 and day 100 for THM1, $k(n)$, $S(n)$ in Figure 4-7. Using the expression $q(r) = q_0 \cdot r_0 / r$, (valid for radial heat transfer) where r_0 is the inner radius of the bentonite block and $q_0 = q(r_0)$, the curve "t = 100 analytical" in Figure 4-7, which corresponds to the total heat flux, is obtained.

A comparison of the analytical and numerical curves shows that the conductive thermal process is correctly handled by Code_Bright, since the curves coincide in the block section, and also that there is another heat transfer mechanism active in the pellet slot as well as in the inner slot. Vapor diffusion acts as a vehicle for the additional heat transfer in these sections, where cycles of evaporation - vapor diffusion – condensation contributes to the heat transfer.

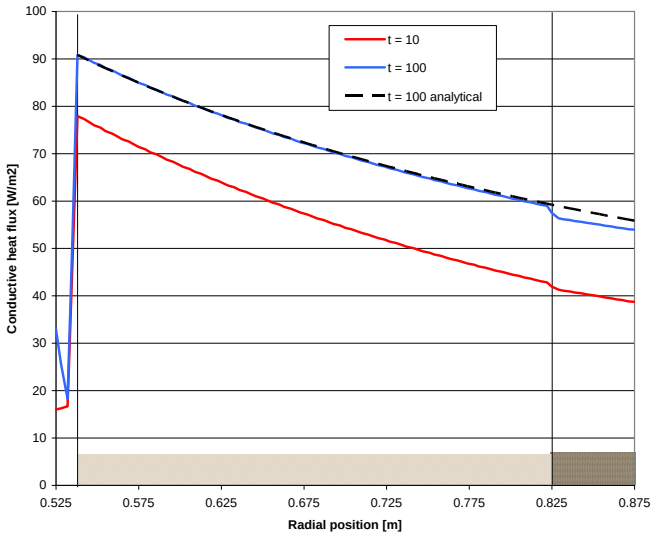

Figure 4-7 ***Simulated conductive heat flux profiles in the buffer after 10 and 100 days and the total, analytically calculated, heat flux at day 100 (hole #1 simulation).***

4.2.2 Hydraulic response

The measured and simulated hydraulic responses are shown in Figure 4-8, Figure 4-9 and Figure 4-10 for r = 0.585, 0.685 and 0.785 m respectively.

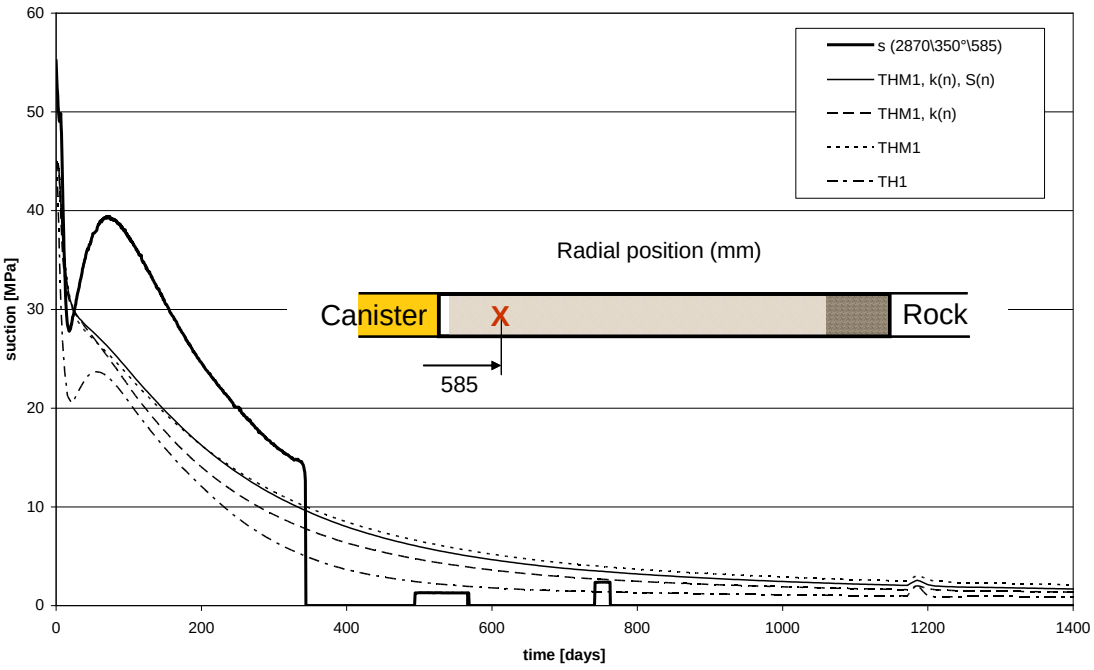

Figure 4-8 ***Measured WBU10013(2.870\350°\0.585) and simulated suction histories at r=0.585 m for hole #1.***

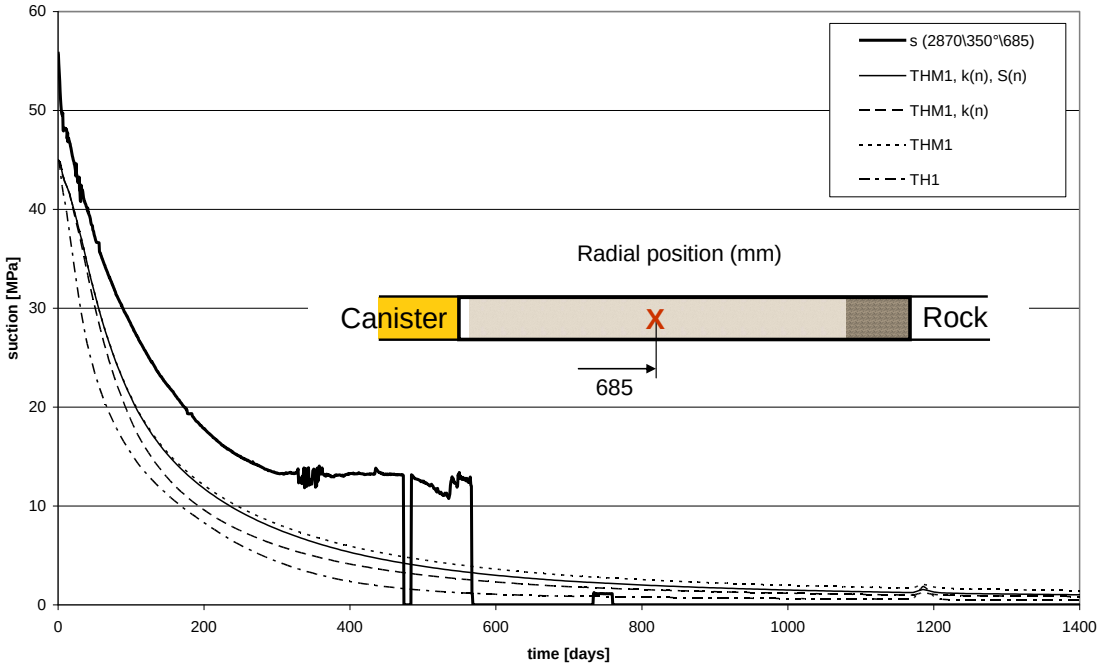

Figure 4-9 ***Measured WBU10014(2.870\350°\0.685) and simulated suction histories at r=0.685 m for hole #1.***

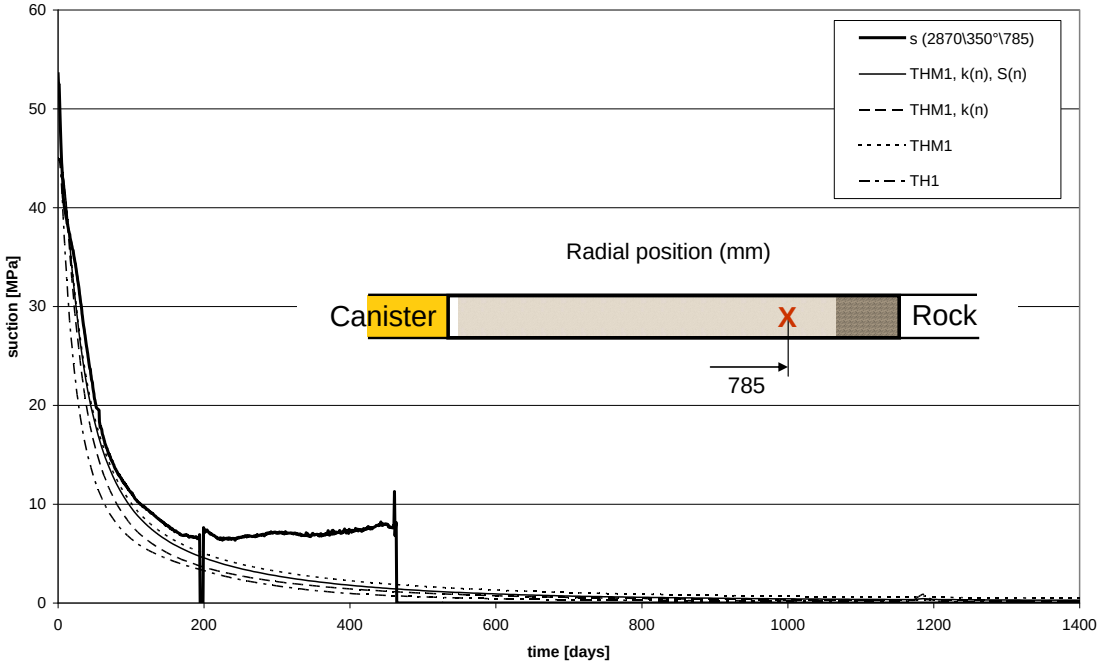

Figure 4-10 ***Measured WBU10015(2.870\350°\0.785) and simulated suction histories at r=0.785 m for hole #1.***

All three sensors break down at some point. The sensors at r = 0.585 m and r = 0.685 m break down after 350 days and the sensor at r = 0.785 m breaks down after 200 days. The data beyond these points is not considered to be reliable. It is also difficult to evaluate the accuracy of the sensor data before the point where the sensors break down.

The simulated responses are all below the corresponding measured one. It should however be remembered that the initial suction of the experiment is 55 MPa as compared to 45 MPa adopted in the model. The reason for this is that in the experiment, locally around the sensors, there are water ratio disturbances which have not been included in the model, c.f. section 0. This could explain part, but not all, of the difference.

The overall trend of the suction responses for the different points is captured. The outer point at r = 0.785 m gives a more rapid decrease in suction (faster wetting) then the point at r = 0.685 m, which in turn has more rapid suction decrease then the point at r = 0.585 m.

The suction response is well reproduced for r = 0.785 m for the interval where the sensor is considered to be working properly. This is however not a result of blind prediction. The response in this point has served as data to calibrate against when determining the value of the leakage parameter in the model. At r = 0.685 m and r = 0.585 m the simulated suction responses are lower as compared to the experimental measurements.

In the three following sections the difference in suction between experiment and simulations is discussed for three aspects:

1. Water saturation
2. Stress state dependent retention
3. Tortuosity and vapor diffusion

1. Water saturation

The simulated low responses of suction at r = 0.685 m and r = 0.585 m indicate that the water saturation is somewhat fast in the model if compared to the measured saturation evolution. The difference between the experiment and simulations might seem considerable for the two inner sensor positions but one should bear in mind that the retention curve is very sensitive to changes in water saturation in the active range. A small difference in water saturation will give a large difference in suction.

In Figure 4-11 the water saturation histories are shown for model THM1 and the experimental measurements. The experimental suction data (and temperature data) has been expressed in water saturation by using the retention function shown in Table 3-6.

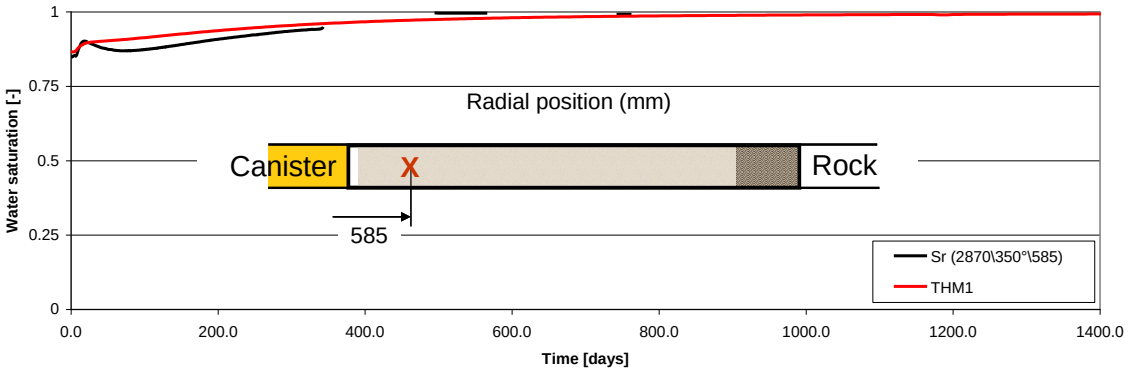

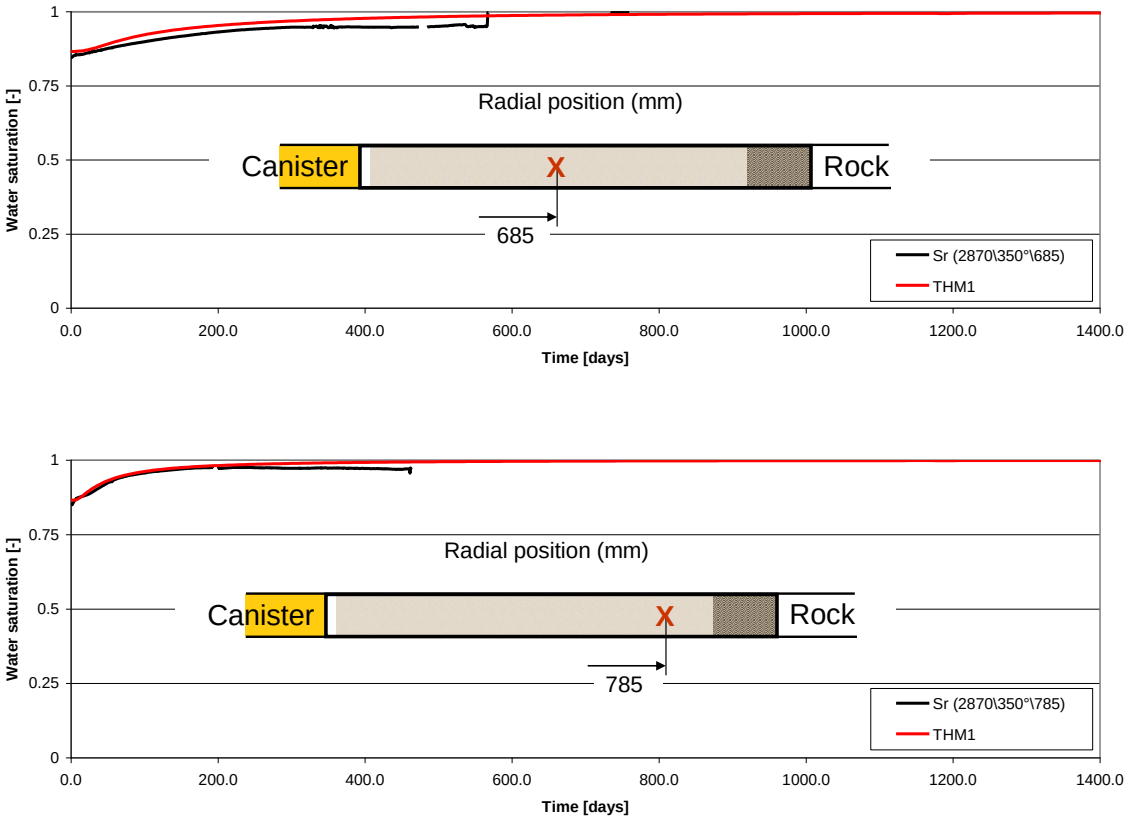

Figure 4-11 ***Experimental and simulated (model THM1) water saturation histories at the different sensor positions (hole #1).***

2. Stress state dependent water retention

Some of the difference between the simulation and the experiment could origin from that the retention model in Code_Bright presently lacks a direct coupling between the stress state and the retention curve which is present in reality.

In Code_Bright the adopted Van Genuchten retention curve expresses the behavior under confined conditions, i.e. the formulation indirect assumes a formulation for the total pressure that has not a coupling to the adopted mechanical model (here BBM). This of course simplifies the formulation since no consideration to the coupling between the stress state and the retention has to be made. On the other hand generality is lost and it is possible to obtain states where the stress state and retention are incompatible. Some coupling is obtained if the option incorporating porosity dependence is used. To evaluate the character of this coupling however, a systematic investigation is needed which is one of the topics suggested for future work.

In the repository there is initially an open inner slot and a soft outer pellet slot that will not give the confined conditions that the used retention curve is valid for. The mechanical homogenization process will take the buffer from a state closer to free swelling than confined conditions in the beginning, to a state closer to confined conditions than free swelling in the end of the process.

This suggests that a stress state dependent retention curve could produce results that would be different as compared to what the present retention curve valid for confined conditions produces. The magnitude of the difference is however not quantified in this report.

3. Tortuosity and vapor diffusion

The difference could also come from unsuitable choices of transport parameter values in the model. The tortuosity of the bentonite is however one transport parameter that is uncertain. If a higher value of tortuosity is used the vapor transportation is more effective from the inner part of the buffer to the outer part and the saturation process will therefore slow down.

To investigate this phenomenon yet a simulation identical to THM1 except for a tortuosity of 1.0 is run. The results from the THM1 simulation using $\tau = 0.15$ and $\tau = 1.0$ and the experimental result are shown in Figure 4-12 for $r = 0.585$ m. For the other radial sensor positions no significant difference was found when changing the tortuosity.

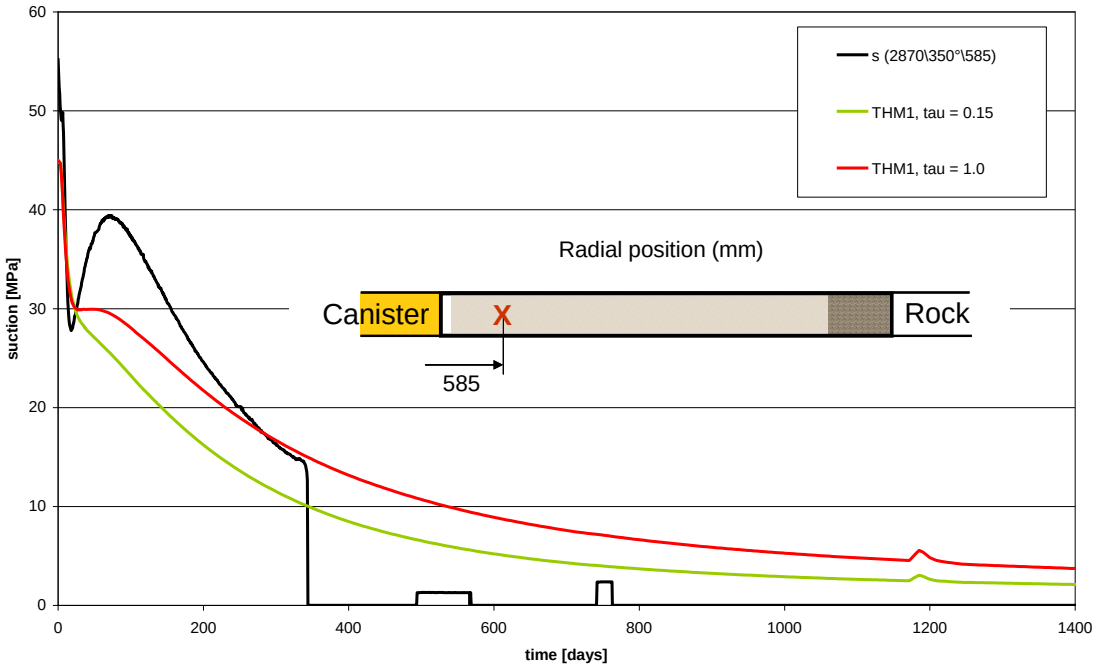

Figure 4-12 ***Measured and simulated suction histories at r=0.585 m for hole #1, when using different tortuosities.***

Increasing the tortuosity gives slower suction decrease in the simulation when the experimental data shows that drying occurs. The drying (suction increase) observed in the experiment is still not captured for the higher tortuosity, but the wetting process clearly slows down considerable at the time when the drying occurs in the experiment. After approximately 300 days the response of the high tortuosity simulation intersects with the measured suction.

The result indicates that this variable only affects the suction evolution in the inner part of the buffer, no significant differences were found for the outer sensor positions, and that a value in the range 0.15 – 1.0 is suitable.

Dependence on homogenization (the mechanical process) and porosity dependent permeability and retention

For $r = 0.585$ m the decrease in suction rate in the initial phase of the simulation is also captured in the models. It is however only the TH1 model that gives an increase in suction, drying, in the initial phase. This difference between the mechanical model THM1 and non-mechanical model TH1 will be studied later in the following section.

The simulated suction responses show that there is a dependence on porosity and the mechanical process. A coarse categorization of the responses of the different models is given by the list below.

1. TH1 gives the most rapid suction decrease.

2. THM1 gives the slowest suction decrease of the investigated models.

3. THM1, $k(n)$ gives faster suction decrease then THM1. The homogenization process makes the bentonite block attain a higher value of porosity which in turn will give higher block permeability. The higher block permeability speeds up the water saturation process.

4. THM1, $k(n)$, $S(n)$ gives a suction decrease that is slower then THM1, $k(n)$ but faster then THM1.

Thus, from the analysis of the suction responses follows that in the investigated time interval (0 - 1400 days):

1. Considering the mechanical process slows down the suction decrease.

2. Including the porosity dependent permeability speeds up the suction decrease.

3. Including the porosity dependent retention slows down the suction decrease.

If instead the time until the entire buffer has more than 96 % or 99 % in water saturation is analyzed the results given in Table 4-4 are obtained.

Table 4-4 ***Time until a specified water saturation is reached in the entire buffer.***

Model name	Time until S_l > 0.96 [years]	Time until S_l > 0.99 [years]
TH1	1.24	1.79
THM1	1.30	3.20
THM1, $k(n)$	1.35	2.20
THM1, $k(n)$, $S(n)$	1.23	5.57

It follows that up to the point where S_l > 0.96:

1. Considering the mechanical process slows down the water saturation.

2. Including the porosity dependent permeability slows down the water saturation.

3. Including the porosity dependent retention speeds up the water saturation.

If the point of interest is when S_l > 0.99 the results are:

1. Considering the mechanical process slows down the water saturation.

2. Including the porosity dependent permeability speeds up the water saturation.

3. Including the porosity dependent retention slows down the water saturation.

The obtained times until S_l > 0.96 are very similar as compared to the case where S_l > 0.99. General and certain conclusions are therefore hard to draw based on the former saturation times.

With this in mind, it can, however, be observed that dependent of which water saturation limit that is considered, different results in the dependence of porosity dependence in the permeability and retention are obtained for the evaluated model. This shows that the rate of the water saturation process is varying with time for the different cases. The water saturation is however slowed down irrespective of which of the water saturation limits that is considered.

Drying in the inner part (a model comparison)

The initial suction response for r = 0.585 m, see Figure 4-8, is here going to be analyzed in detail for TH1 and THM1. The initial rapid suction decrease, for the first 20 days, is captured in both cases. The response of TH1 shows the largest initial decrease in suction of all the cases. The following increase in suction, the drying process, measured in the experiment is only obtained for TH1.

To investigate the origin of the difference in the suction responses corresponding to mechanical and non-mechanical simulations, an expression of the suction rate (at a given material point of the buffer and at a given time) has been derived. The suction has in the derivation been considered a function of water saturation and temperature only according to the "pure" Van Genuchten without dependency on the porosity. See appendix for more information about the derived expression. The expression reads

$$\dot{S} = \frac{\partial S(S_l,T)}{\partial S_l}\dot{S}_l + \frac{\partial S(S_l,T)}{\partial T}\dot{T}\,, \tag{10}$$

where the ingoing water saturation rate can be expressed as:

$$\dot{S}_l = \frac{1}{\rho_l e dV_s}(\dot{dm_w^l}) - \frac{S_l}{\rho_l}\dot{\rho}_l - \frac{S_l}{e}\dot{e} \tag{11}$$

In (10) and (11) the dots indicate the material time derivative $\partial(\,)/\partial t$ and dm_w^l denotes the mass element of liquid water at the material point considered. As (10) and (11) shows the rate of suction may be considered to depend on rates of liquid water mass, water density, void ratio and temperature. The coefficients in (10) are always negative in the active ranges of S_l and T, see appendix, so positive rates in water saturation and temperature gives a negative suction rate.

Below in Figure 4-13 (10) is represented for r = 0.585 m for TH1 and THM1. For THM1 the retention curve and permeability is not porosity dependent. In the graphs the suction rate and the two terms in (10) are shown for the first 100 days of the simulation.

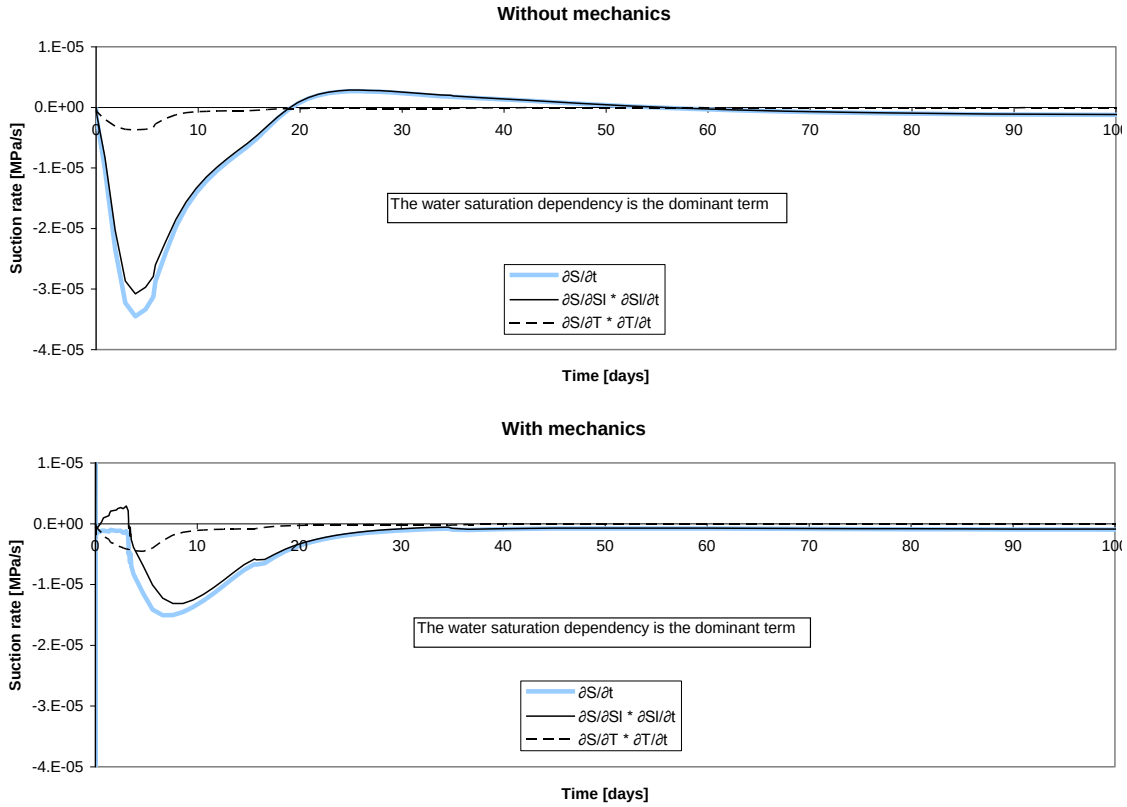

Figure 4-13 ***Suction rate and the suction rate components at r = 0.585 m for TH1 and THM1 (hole #1 simulations).***

The suction rates naturally reflect what was seen in the suction responses. The response of TH1 shows an immediate reaction of a negative suction rate whereas the response of THM1 has a slower response of less negative suction rate.

When studying the components of the suction rate it can be seen that in TH1 both components acts for a negative suction rate. For THM1 however, the water saturation rate term in (10) is positive in the first four days and counteracts a suction decrease. Between day 4 and day 15 the absolute value of the water saturation rate term is lower for THM1 as compared to TH1.

At approximately day 20 the suction rate becomes positive for TH1 which means that drying occurs. As discussed before, the response of THM1 does not have any drying which also the suction rate curve reflects by not attaining any positive values.

As Figure 4-13 shows the first term in (10), i.e. the water saturation rate term, is dominant and governs the suction rate for both cases.

The second term of (10) contains a variable coefficient that is dependent on both temperature and water saturation. Since the temperature responses are similar for both TH1 and THM1 case the water saturation is the variable that is responsible for the different responses.

To investigate the water saturation evolution further (11) is used. Plotting the result obtained using (11) for the two investigated cases gives Figure 4-14. In a similar fashion as for the suction rate the water saturation rate is shown together with it's components given by (11). Also here the first 100 days of the simulation is shown.

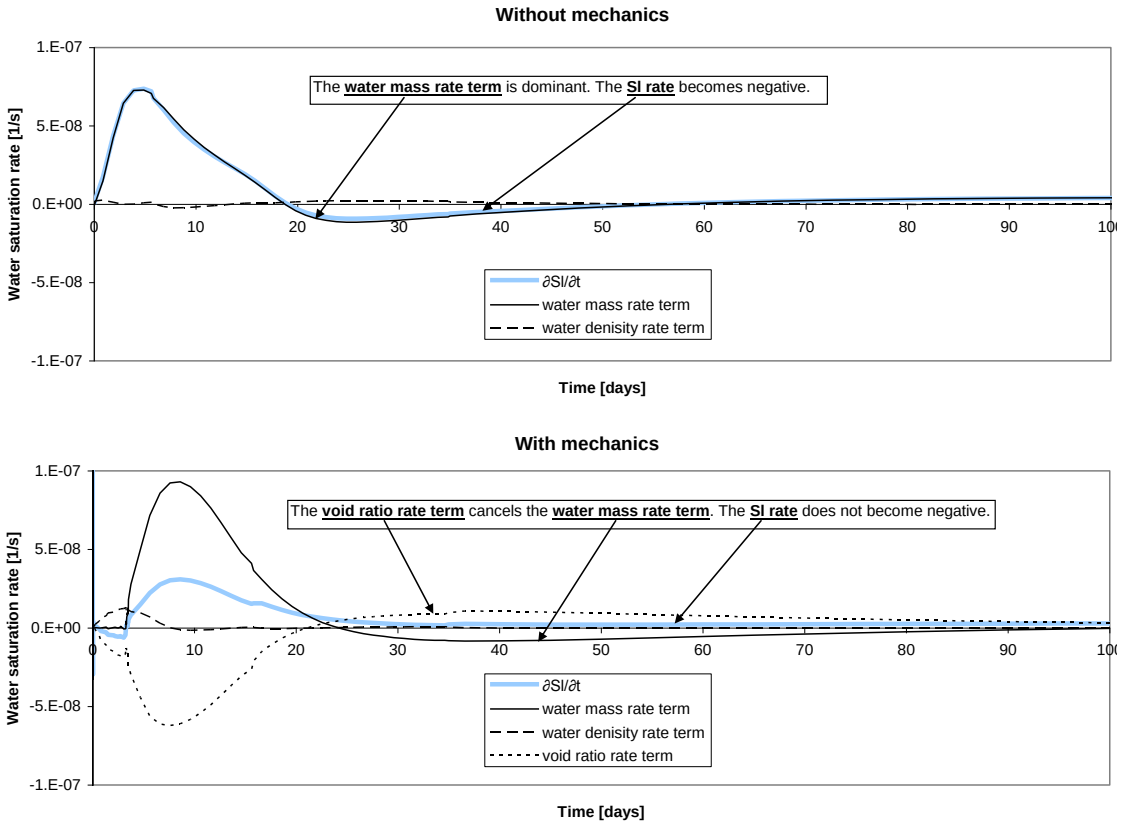

Figure 4-14 ***Water saturation rate and water saturation rate components at r = 0.585 m for TH1 and THM1 (hole #1 simulations).***

For TH1 the process is straight forward where the water saturation rate can be seen to be dominated by the water mass rate term (the first of the terms in (11)). When the mechanics is considered as in THM1 the void ratio term also plays an important rule.

Studying the response of THM1, it can be seen that for the first 4 days the water mass rate term is small as compared to the other two components. It can also be seen that the void ratio rate term and the water density rate term counteracts and as a consequence the water saturation rate becomes very small for this initial phase.

From 4 days and up to approximately 16 days the water saturation rate is lower for THM1 as compared to TH1. If the components of the water saturation rate for THM1 are investigated it can be seen that the water mass rate term actually is larger for a large part of the time interval as compared to the same response for TH1. The void ratio rate term is however working against the water mass rate term for THM1 and the sum of the both add up to a lower value as compared to what the TH1 gives.

This is also what makes the water saturation rate never to become negative for THM1. The water mass rate term and the void ratio term never add up to a negative value. No drying will therefore occur for the present model setup (for the parameter values and boundary conditions chosen) when the mechanical process is considered.

4.2.3 Mechanical response

Axial stress

The mechanical response in terms of axial stress is well reproduced quantitatively, see Figure 4-15. There is a significant dependency on presence of porosity dependency in the retention and permeability in the stress response. The measured stress starts to build up first after

approximately 100 days in contrast to the simulations where the stress build-up starts immediately. The sudden drop down to zero stress, just before 1200 days in the experiment, most likely comes from the drop in temperature when the heaters were shut down at this instant. The models do capture this thermal stress relaxation, but not to the extent as measured in the experiment.

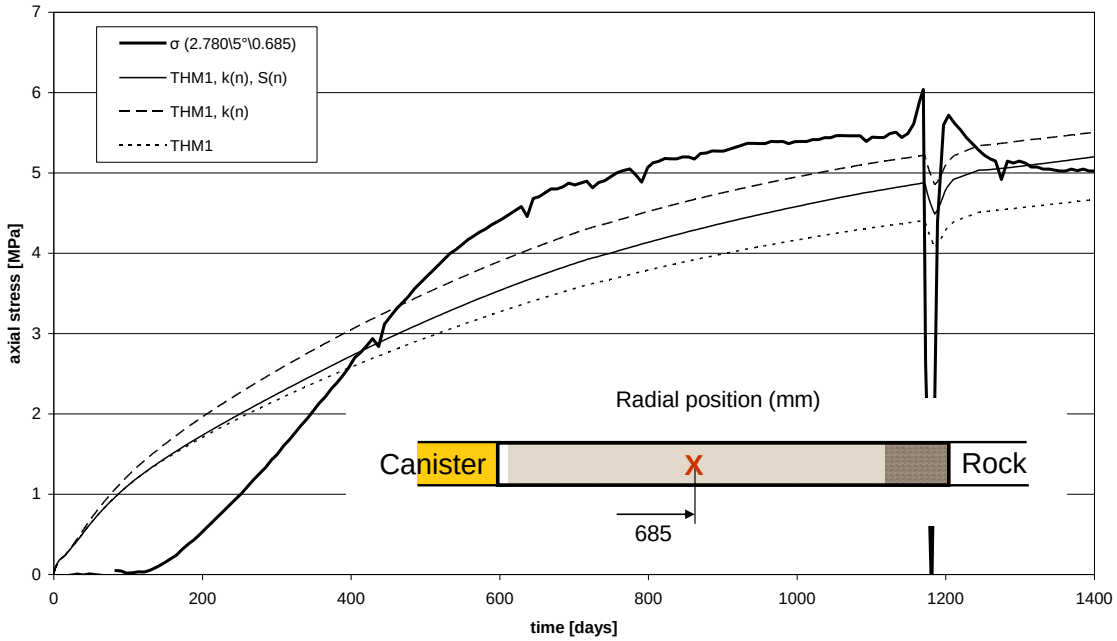

Figure 4-15 ***Measured PBU10011(2.780\5°\0.685) and simulated axial stress history for hole #1.***

Figure 4-15 shows that THM1 gives faster stress buildup as compared to THM1, *k*(*n*), *S*(*n*) which in turn gives faster stress buildup as compared to THM1, *k*(*n*). This is a direct consequence of the different suction evolutions.

In the mechanical material model there is a direct coupling between the suction rate and stress rate, which can be seen in Table 3-9. When considering of how they relate in the constitutive law a hydrostatic confined experimental setup can be imagined. When the suction rate is negative, $dS < 0$ the pressure increment will be positive, $dp' > 0$, under the imagined confined conditions. Thus, wetting gives a swelling pressure.

The conditions are more complex than being confined in the simulations performed here but the result of the discussion using the imagined simple experimental setup above still holds. Faster decrease in suction gives faster stress buildup.

The slow start of the stress build up in the experiment probably comes from the presence of low-density volumes around this pressure sensor. Such low-density volumes around the sensors may appear when the necessary degree of compaction of the bentonite powder, used to backfill the cavities around the sensors, is not reached at installation. The low-density volume around the sensor therefore needs to be homogenized before any pressure will develop in the experiment. In the model, the material is considered to be homogeneous in the blocks and the effect from low-density volumes will therefore not be captured in the simulation.

Void ratio profiles

The simulated void ratio profiles at full water saturation (here the problem was simulated for 16.4 years (6000 days) to be sure of that a fully water saturated state was obtained) shown in Figure 4-16, have the same overall features as the void profile of the CRT experiment shown

in Figure 4-17, see /Johannesson, 2007/. Going from left to right (from the canister towards the hole wall) the void ratio is first slightly decreasing due to the initial presence of the inner slot. Further to the right the void ratio starts to increase up to where the block/pellet slot interface is positioned, and after the transition from the block to the (former) pellet slot the void ratio levels out.

The pellet slot elastic parameters were calibrated so that a “smooth” and “continuous” void ratio profile was obtained for the base case setup. I.e. the void ratio profile should not have abrupt changes at the interface between the bentonite block and pellet slot. There is a dependency on presence of porosity dependence in the constitutive laws in the void ratio profiles in the pellet slot section.

In the figures showing the void ratio profiles of the simulation and the CRT experiment the initial void ratio as well as the homogenized initial void ratio are shown. It can be seen that the simulated void ratio profiles can be considered to be in the right void ratio range as compared to the corresponding homogenized initial void ratio when comparing with CRT data. In Figure 4-17 the homogenized void ratio of the current void ratio profile, i.e. the shown data points, is also shown. The homogenized current void ratio is slightly higher as compared to the homogenized initial void ratio.

Also here the different rates of decrease in suction can be seen to give different void ratio profiles since the stress buildup, investigated above, will compress the pellet slot to different extent.

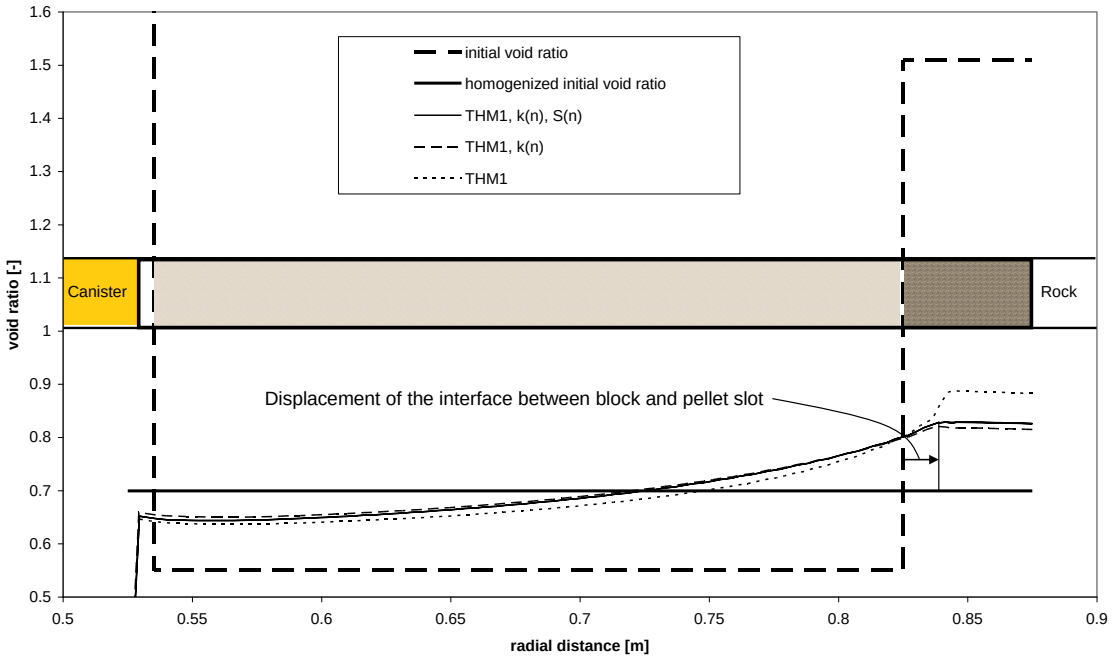

Figure 4-16 ***Simulated void ratio profiles at full water saturation (here after 16.4 years) for hole #1.***

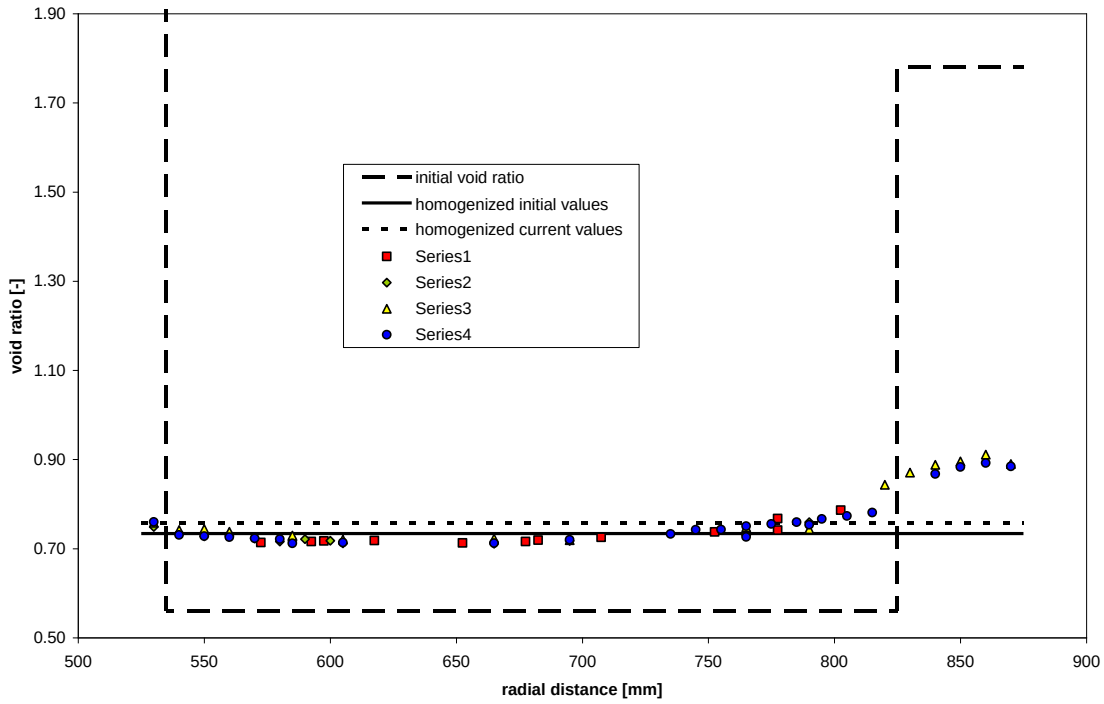

Figure 4-17 ***CRT void ratio profile at Ring 7 (second ring above canister mid-height).***

4.3 Hole #3 (dry conditions)

Here the Base Case, THM1, $k(n)$, $S(n)$, of hole #1, equipped with a new set of boundary conditions, thermal and hydraulic, that corresponds to the thermal 3D simulation and the sensor data for hole #3, defines the Base Case for hole #3, denoted THM3, $k(n)$, $S(n)$, of hole #3. In this way the generality of the model is tested, in the sense how well the model can simulate the buffer system subjected to different thermal and hydraulic conditions with the same set of material parameters. The case where the mechanical process is omitted, denoted TH3, is also used to see the influence from the mechanical process under dry conditions. The models used are shown in Table 4-5 and the sensors used when comparing the simulations with the measurements are identified in Table 4-6.

Table 4-5 ***Overview where the models used for hole #3 are characterized.***

Model name	Elements	Mechanics	$k(n)$	$S(n)$
THM3, $k(n)$, $S(n)$	1×103	X	X	X
TH3	1×103			

Table 4-6 ***Sensor label, position and measured variables for the sensors used for the comparisons made in hole #3.***

Sensor label	WBU30013	WBU30014	WBU30015	PBU30011
Sensor position ($z\backslash\alpha\backslash r$)	(2.840\350°\0.585)	(2.840\350°\0.685)	(2.840\350°\0.785)	(2.771\5°\0.685)
Measured variable	*RH, T*	*RH, T*	*RH, T*	σ_a

4.3.1 Thermal response

As for hole #1 the reproduced temperatures are slightly lower as compared to the measured as shown in Figure 4-18. Also in this case the adopted boundary conditions are probably one of the causes of the difference. Omitting the mechanical part of the model does not affect the thermal response significantly.

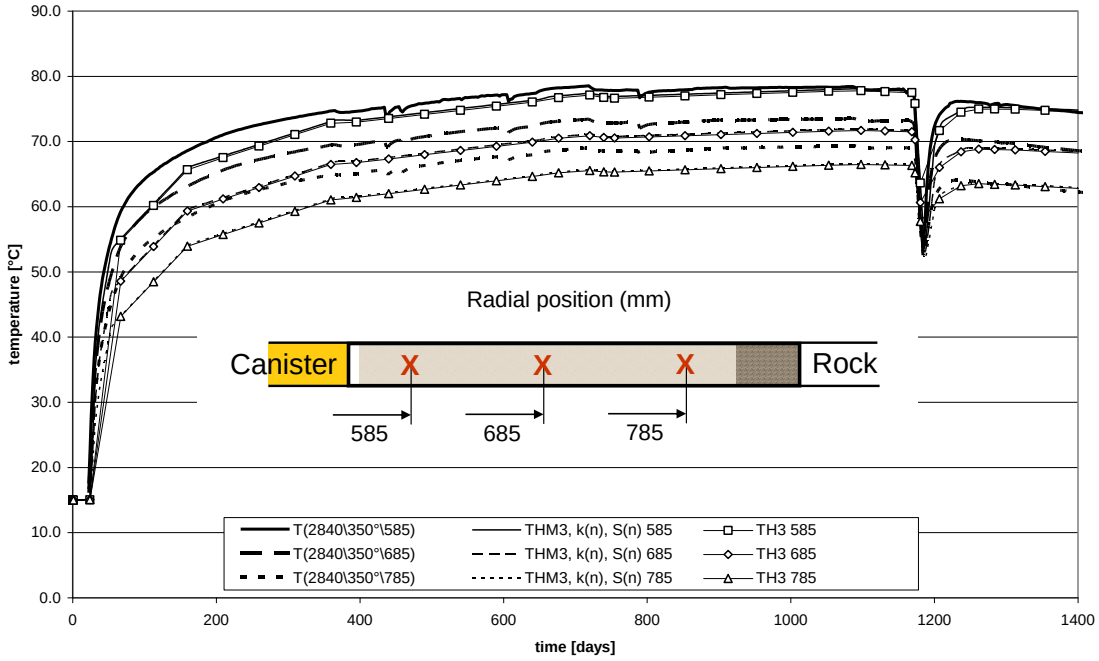

Figure 4-18 ***Measured and simulated temperatures in the buffer material in hole #3.***

One character that differs from the simulation of hole #1 is that the difference between the measured and simulated temperatures increases with the radial position. In hole #1 the difference was relatively constant with the radial position.

To investigate this phenomenon closer, temperature profiles obtained from the measurements are compared with simulated temperature profiles at approximately 100 days and 400 days. In Figure 4-19 the measured and simulated temperature profiles are shown.

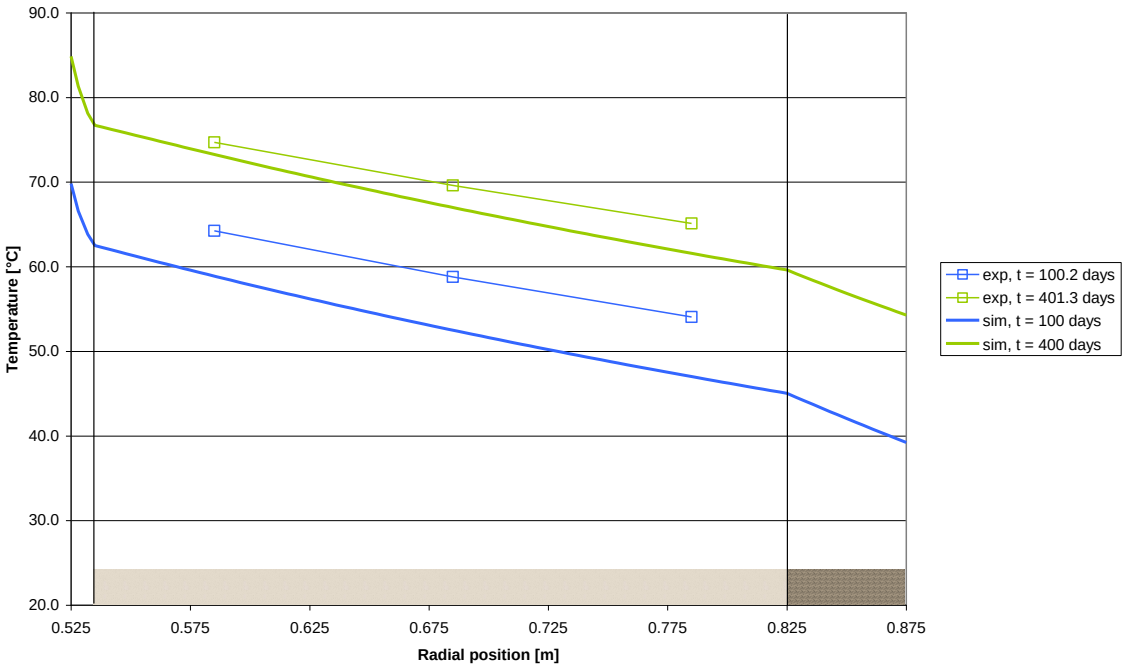

Figure 4-19 ***Measured and simulated temperature profiles in the buffer at day 100 and day 400 (hole #3).***

As can be seen in Figure 4-19 the temperature gradient does not match as well as in hole #1, see Figure 4-6. Thus the ratio between radial heat flux and the bentonite block conductivity, q_0/λ_b, is too high in the simulation.

The heat flux used in the hole #3 simulation has already been investigated in section 3.3.1, where the bentonite conductivity was calculated from the heat flux and the measured temperatures at day 395. It was concluded that the heat flux probably is prescribed too high in hole #3 and that the bentonite block conductivity used in the model is somewhat low as compared to what was obtained in the study and also as compared to experimentally measured values in lab-scale, see Figure 3-2.

As discussed earlier in section 0, where the temperature in hole #1 were examined, the deviation in heat flux could stem from that heat transportation is inhomogeneous in the experiment which has not been considered in the 3D model. In the developed 3D model from which the heat-flux were obtained, ideal positioning of the canisters (where the center-line coincides with the center-line of the hole) has been assumed as well as homogeneous conductivity in the buffer and rock mass.

Scenarios where those assumptions are violated would produce an inhomogeneous field of heat-flux where a lower heat-flux, as compared to the ideal model, could be obtained at different locations.

4.3.2 Hydraulic response

The order of the curves corresponding to the different radial distances is the same in the simulation and the experiment, which are shown in Figure 4-20. Also here, when omitting the mechanical process, the curves are lowered.

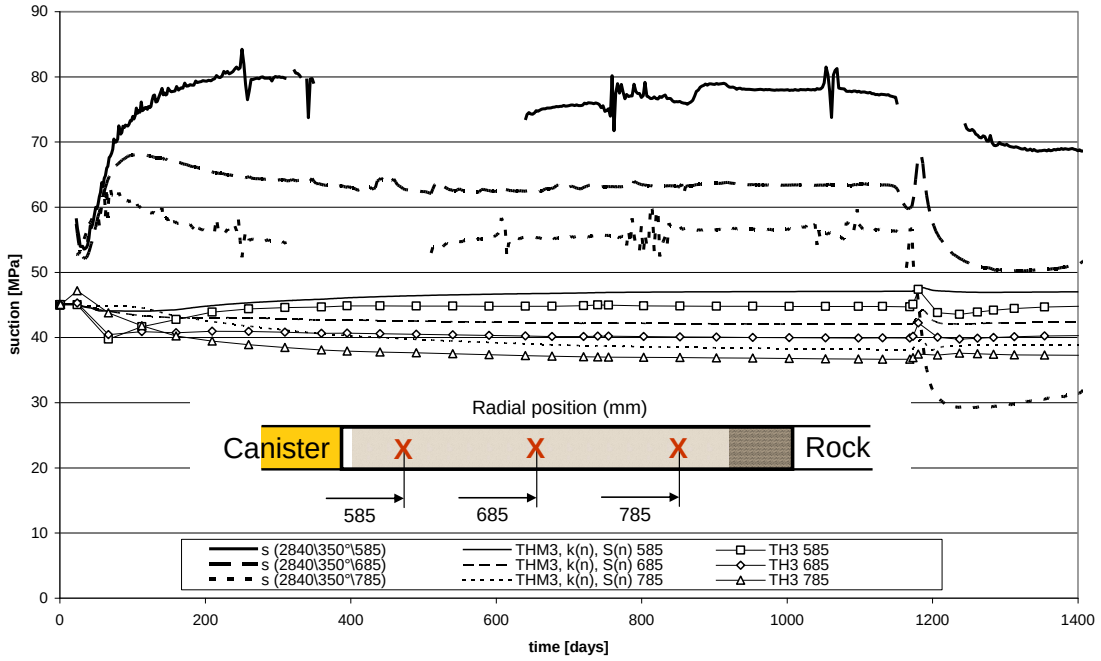

Figure 4-20 ***Measured and simulated suction histories for hole #3.***

The difference between the experiment and simulation could come from that the used leakage coefficient is not optimized. However, the discrepancy between the experiment and the simulation may seem significant but the sensibility of the retention curve magnifies the water saturation difference when translated into suction, which also was discussed for hole #1 in section 4.2.2. As an example, a suction of 50 MPa, approximately as in the simulation, corresponds to a water saturation of 0.855 and a suction of 80 MPa, approximately as in the experiment, corresponds to a water saturation of 0.805 with the adopted retention curve for the bentonite block. Thus, the apparent large difference between the experiment and simulation in suction is not that significant when translated in water saturation.

This can also be seen in Figure 4-21 where the experimental suction responses have been translated into water saturation by using the retention relation without porosity dependence. In Figure 4-21 the responses of THM3, $k(n)$, $S(n)$ are also shown.

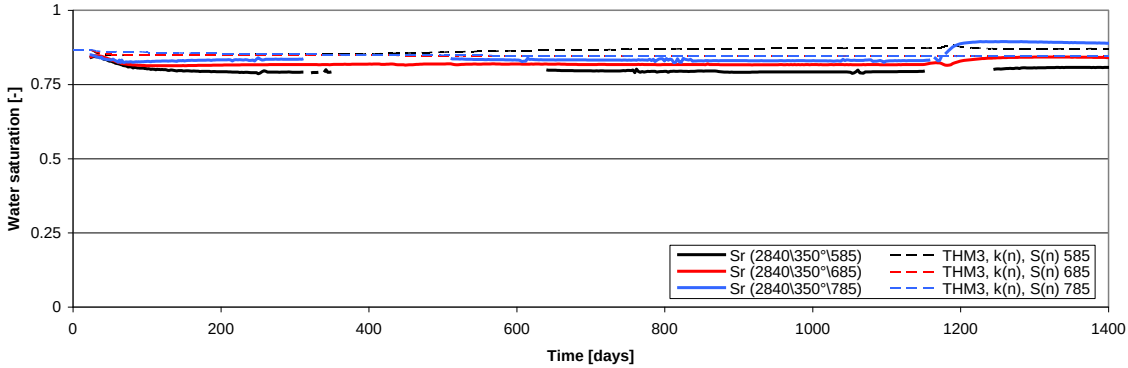

Figure 4-21 ***Measured and simulated water saturation histories for hole #3.***

4.3.3 Mechanical response

Since the water inflow is very low in hole #3 the buffer will not swell and create such large magnitude of axial stress as in hole #1. Figure 4-22 shows that the stress magnitude of the simulation corresponds well with the measured stress with the parameters obtained from the calibration made in hole #1.

Here, both experimental and simulated responses react fast. The stress begins to increase before day 50. Thus, for this sensor, no effect from low-density volumes, as is thought to prevail at the corresponding sensor in hole #1, can be observed.

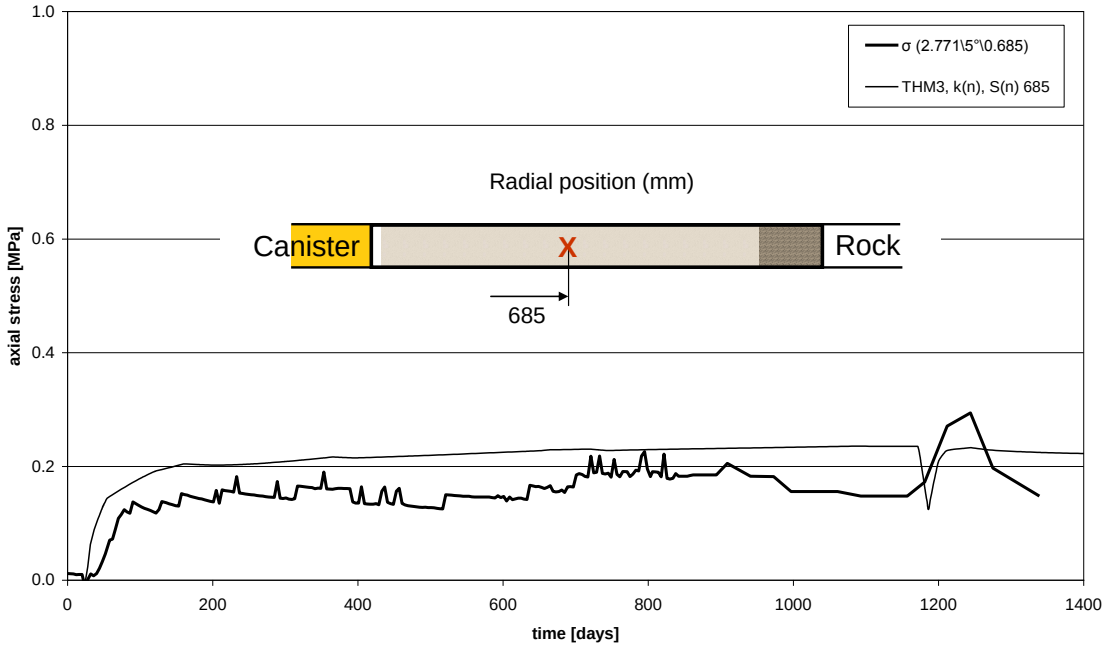

Figure 4-22 ***Measured and simulated axial stress history for hole #3.***

5 Conclusions and comments

Here the THM-processes in the buffer at canister mid-height of hole #1 and #3 have been investigated by performing simulations of 1-D radial models using the finite element solver Code_Bright. The code provides possibilities for solving coupled THM problems where a poro-mechanical approach is used. The simulations have been compared with measured histories of temperature, suction and stress.

The model is equipped with material parameter values mostly obtained from laboratory experiments. When simulating different deposition holes the material parameters are not altered. The model is only adjusted to different deposition holes by adopting different boundary conditions corresponding to the conditions that prevail at the hole considered.

To be able to capture the mechanical homogenization of the buffer, when the bentonite clay swells due to water uptake, it was found that the bentonite block material and the pellet slot material had to be allotted with different mechanical parameter values.

The parameter values of the bentonite block have been prescribed according to what has been found when studying experimental findings.

The pellet filled slot has been considered as a homogenous material in the model. Since there was a lack of information about the mechanical properties of the pellet filled slot, the mechanical parameters of the pellet slot were calibrated using the experimental stress history in hole #1 and the void ratio profile at full water saturation obtained in the CRT experiment.

The canister heat flux used as a boundary condition in the 1D-THM model was obtained from the thermal 3D model discussed in /Kristensson and Hökmark, 2007/. An evaluation of the canister heat flux has here been performed by comparing the obtained bentonite block conductivity, from using measured temperatures and calculated canister flux, with experimental findings. This investigation indicated that the simulated heat flux of canister #1 was in good agreement with the experiment and that the simulated heat flux of canister #3 overestimated the heat flux in the experiment. The analysis also indicates that the experimental findings on the laboratory scale are valid on the buffer scale.

The ratio between the bentonite block conductivity and pellet slot conductivity has been studied using measured temperatures in hole #5 and hole #6. The obtained best estimate of the initial pellet slot conductivity, using an initial bentonite block conductivity of 1.2 W/(m·K), was 0.29 W/(m·K).

5.1 Model generality

The generality of the entire model, in terms of being able to represent different deposition holes using different boundary conditions only, could be studied performing a “blind” prediction of the behavior of deposition hole #3, where reasonable agreement with the experiment was obtained. The character of the suction (or water saturation) and stress history are captured using the model.

The mechanical material model (BBM) reproduces the buffer behavior well. A void ratio profile (transecting the block as well as the pellet slot) that agreed well qualitatively (and reasonably well quantitatively) with corresponding measurements made after dismantling of the CRT experiment, i.e. at full water saturation, can be obtained. This means that the model captures the expansion of the high density blocks and the compression of the low density slot well.

The model is not general enough to capture the block behavior and the pellet slot behavior with one single set of model parameter values. For the slot material, extensive and time consuming calibration efforts were necessary. No lab scale results from low-density lab scale samples are available.

In this work only the elastic part of BBM has been tried. At present it is not clear if the full elasto-plastic model would be capable of capturing the behavior of both materials with one single set of model parameter values, even given that the experimental background data would be sufficient to allow for a systematic calibration of all model parameters, including those associated with the plastic behavior.

Another part of the model that has shortcomings in term of generality is the coupling between the retention (suction) and the stress state. The formulation implemented in Code_Bright, irrespective of whether the elastic BBM or some other mechanical model is used, is tailored for confined conditions, which indirectly generates an implicit formulation of the stress evolution which is decoupled from the mechanical state of the model used. For the presently studied problem the conditions are close to free at the initial state, where there is an open slot at the canister side and a pellet-filled slot with low density at the hole wall side. When the buffer swells the inner slot closes and the pellet-slot becomes more compacted, and consequently, the conditions become close to confined.

A possible drawback with using a formulation with a more direct coupling between the stress state and the suction is that it would require a mechanical model that represents the material with a very high accuracy in order not to produce corrupted results. Since the mechanical behavior of bentonite is difficult to model it could therefore demand considerable efforts to develop such a model.

5.2 Dependency on homogenization and porosity

The temperature response was found to be insignificantly dependent on the mechanical process (the homogenization). Also explicit dependence on porosity in the constitutive relations of the retention and liquid water flux (the permeability parameter) did not give a significant change in the temperature responses.

The hydraulic response was found to be dependent on the mechanical homogenization. When incorporating the mechanics the wetting process slowed down. The times until the entire buffer had over 96 % or 99 % water saturation in the entire buffer in hole #1 are given in the table below. TH1 denotes the Thermo-Hydraulical model and THM1 the Thermo-Hydraulic-Mechanical model respectively.

Model name	Time until S_l > 0.96 % [years]	Time until S_l > 0.99 % [years]
TH1	1.24	1.79
THM1	1.30	3.20

When investigating the influence of incorporating a porosity dependency in the retention curve and permeability in terms of time until 96 % or 99 % water saturation in the entire buffer the results shown in the table below was obtained. $k(n)$ indicates that the permeability is porosity dependent and $S(n)$ that the suction is porosity dependent.

Model name	Time until S_l > 0.96 % [years]	Time until S_l > 0.99 % [years]
THM1, $k(n)$	1.35	2.20
THM1, $k(n)$, $S(n)$	1.23	5.57

When comparing the results above with THM1 it can be found that the including the porosity dependent permeability or including both porosity dependent permeability and retention have different effects for the two chosen water saturation limits. Thus, the rate of the water saturation process changes with time for the different cases investigated

Since the stress buildup is dependent on the suction rate the stress histories will only reflect what was discussed about the water saturation above in terms of dependence on porosity dependence in suction and permeability. In the simulation of hole #1 the difference in axial stress at day 1400 (the time at the end of the simulations) is approximately 1 MPa between the most diverging solutions which are approximately symmetric around 5 MPa.

5.3 Thermal response

The temperature responses are reasonable represented for both hole #1 and hole #3 simulations. The temperatures were however found to be underestimated in the simulations of both holes.

A number of possibilities that lead to an underestimation can be thought of:

1. The rock temperature is too low.
2. The pellet slot conductivity is too high.
3. A combination of too low canister heat flux and too low block conductivity.
4. The radial assumption is not valid due to non-radial contributions.

These error-sources are discussed in the context of the present simulation in section 0.

For hole #3 the temperature gradient does not match as well as for hole #1. The temperature gradient is too high in the hole #3 simulation. The reason for this is believed to come from that the radial heat flux is prescribed too high in the simulation and that the bentonite conductivity is underestimated in the model.

The mechanisms that contribute to the heat transfer in the simulation have been found to be conduction and also convection due to vapor diffusion in the inner and pellet slot.

5.4 Hydraulic response

The hydraulic behavior, in terms of suction or water retention, is reasonable reproduced. The initial wetting-drying cycle present at the inner sensor position in hole #1 is only obtained for the non-mechanical simulation with the presently used parameter set.

In the experiment the holes where the hydraulic sensors were placed were backfilled with bentonite powder of lower water ratio as compared to the surrounding block. Since these local disturbances could not be included in the model, the initial state of the bentonite block material is too wet in the simulations which could explain some of the discrepancy between model and experiment.

5.5 Mechanical response

The axial stress responses are in agreement with the measured data. The similarity between experiment and simulation for hole #1 is not, as mentioned above, accomplished by a blind prediction, since the pellet slot parameters were calibrated using this data. But the similarity in the responses for hole #3 indicates that the chosen parameter values are suitable. For hole #1 the late stress buildup in the experiment probably comes from the presence of low-density volumes or voids around the pressure sensor which has not been considered in the model.

The simulated void profiles at full water saturation have the same trend as the void profiles of the CRT experiment. When comparing the position of the void profiles, at full water saturation, relative to the homogenized initial void profile in the simulation and the CRT experiment, the magnitude of the void ratio also seems reasonable. It is stressed that also here, exactly as for the stress history, the result is not obtained by a blind prediction for hole #1. The result, however, proves that it is possible to calibrate the material parameters so that the model can capture the homogenization process as well as the stress evolution in the buffer in a reasonable way.

5.6 Future work

The next natural step in the sequence for modeling the Prototype Repository experiment is to expand the model geometrically to incorporate an entire deposition hole. For this purposes an axisymmetric 2D model would be suitable to start with. To begin with, only the TH processes could be incorporated to investigate the saturation process and if this study turns out well the mechanical process could also be considered.

Using such an axisymmetric 2D model the influence from inhomogenity in the boundary conditions as well as in the material properties could be studied. Also the inhomogenity in the axial direction due to the geometric asymmetry in this direction is possible to be captured.

One could also develop a plane 2D model of a horizontal cut through the canister and buffer at canister mid height. If this model is equipped with the boundary conditions and material properties used for the 1D model this 2D model is equal to the 1D model used in the present study. But if heterogeneous boundary conditions and/or material properties are used there is a possibility to study heterogeneous processes in the horizontal plane.

The influence from using a refined mechanical model by including the plasticity in BBM would be of interest. A more radical, but maybe necessary, change of the mechanical model, where a new formulation is implemented in the code, might be the most satisfying path to go in order to obtain a model where the coupling between density and swelling pressure at full water saturation is correctly captured.

The indirect coupling to the stress state in the retention curve, when incorporating dependence on porosity, is of interest to categorize.

It would also be of interest to evaluate how a model where an explicitly stress state dependent retention relation is used influences the hydraulic response. This would need development of a suitable formulation and implementation of the new retention relation in the code.

6 References

Alonso E E, Gens A, Josa A, 1990. *A constitutive model for partially saturated soils. Géotechique 40, No. 3, 405-430.*

Birgersson M, Åkesson M, Hökmark H, Lönnqvist M, 2007*. Engineered Barrier System Task Force:Calculation of benchmark 1.1.1. Clay Technology Report to Äspö Hard Rock Laboratory International Joint Committee.*

Börgesson L., Hökmark H. and Karnland O., 1988. *Rheological properties of sodium smectite clay, SKB TR-88-30.*

Börgesson L., Johannesson L.-E., Sandén T. and Hernelind J., 1995*, Modelling of the physical behavior of water saturated clay barriers. Laboratory tests, material models and finite element application, SKB TR-95-20.*

Börgesson L. and Hernelind J., 1999*. Coupled thermo-hydro-mechanical calculations of the water saturation phase of a KBS-3 deposition hole. Influence of hydraulic rock properties on the water saturation phase. SKB TR-99-41.*

Börgesson L., Gunnarsson D., Johannesson L. and Sandén T., 2002*. Prototype Repository, Installation of buffer, canisters, backfill and instruments in Section 1. SKB IPR-02-23.*

CIMNE, 2004. *Code_Bright. Version 2.2 users guide. Departemento de Ingenieria del Terreno, Cartográfica y Geofísica. Universidad Politécnica de Cataluña.*

Dueck A., 2004. *Hydro-mechanical properties of water unsaturated sodium bentonite. Laboratory study and theoretical interpretation. PhD thesis. Division of Soil Mechanics and Foundation engineering. Lund Institute of Technology, Lund University and Clay Technology AB.*

Goudarzi R. and Johannesson L.-E., 2007. *Sensors data report (Period 010917-070601) Report No:17. IPR-07-19*

Hökmark H., Sundberg J., Kristensson O. and Lönnqvist M., 2008. *Strategy for thermal dimensioning of the final repository for spent nuclear fuel. (in preparation)*

Johannesson L.-E., 2007*. Testing of a retrieval technique, Dismantling and sampling of the buffer and determination of density and water ratio. SKB IPR-07-16.*

Kalbantner P. and Johannesson L.-E., 2000. *Hållfasthetsberäkningar för en bentonitbuffert bestående av enaxligt kompakterade bentonitkroppar, SKB R-00-42.*

Kristensson O. and Hökmark H., 2007*. Thermal 3D modeling of Äspö Prototype Repository. SKB IPR-07-01.*

Ledesma A., Chen G. J., T-H-M, 2003*. Modelling of the prototype repository experiment. Comparison with current measurements. Proceedings of the international symposium on large scale field tests in granite – Barrier behavior and THM modelling, Sitges, Barcelona, Spain, 12-14th November.*

Rhén I., and Forsmark T., 2001. *Hydrogeology, Summary report of investigations before the operation phase. SKB IPR-01-65*

***SKI, 2005**, SKI:s yttrande över SKB:s redovisning av FUD-program 2004, SKI Report 2005:31.*

***Sugita Y., Chijimatsu and Suzuki H., 2003**. Fundamental properties of bentonite pellet for prototypr repository project, Proceedings of the international symposium on large scale field tests in granite – Material behavior and laboratory testing, Sitges, Barcelona, Spain, 12-14th November.*

***Åkesson M, 2006**. Äspö Hard Rock Laboratory. Temperature Buffer Test. Evaluation modeling. TBT_3 Mock-up test. SKB IPR*

Appendix A - Calculating the suction rate

When investigating the influence of mechanics on suction, the suction change in the considered material point, with the position vector $\boldsymbol{X}$ in the reference, is investigated at time t. At $\boldsymbol{X}$ a volume element is defined $dV = d\beta\, dz\, dr\, 2r$ in terms of increments of the cylindrical coordinates with obvious notation. The volume element is divided into dV_s, the solid volume element and dV_p, the pore volume element. dV_p is further divided into dV^l, the liquid volume element and dV^g, the gas volume element. The liquid volume element is in turn split into $dV_w^{\,l}$ and $dV_a^{\,l}$, the liquid water and liquid air (dissolved air) volume element respectively.

The material time derivative of the suction field, $S(\boldsymbol{X},t)$, is defined below where it also is related to the suction increment dS and time increment dt.

$$dS(\boldsymbol{X},t) = \frac{\partial S}{\partial t}dt = \dot{S}dt \tag{A1}$$

In (A1) the dot indicates the material time derivative.

The relations shown in (A2) – (A6) are used when deriving an expression for the suction change.

$$S = S(S_l,T) \tag{A2}$$

$$S_l = dV_w^{\,l} / dV_p \tag{A3}$$

$$dm_w^{\,l} = \rho_l\, dV_w^{\,l} \tag{A4}$$

$$e = dV_p / dV_s \tag{A5}$$

$$n = dV_p / dV \tag{A6}$$

(A2) is the retention relation, here Van Genuchten shown in Table 3-6. As a point of departure the material time derivative operate on (A2), i.e.

$$\dot{S} = \frac{\partial S(S_l,T)}{\partial S_l}\dot{S}_l + \frac{\partial S(S_l,T)}{\partial T}\dot{T} \tag{A7}$$

The coefficients in (A7) are shown in Figure A1 where they are plotted against the water saturation, $S_l \in \{0.8, 1.0\}$, for T = 15 °C and T = 65 °C.

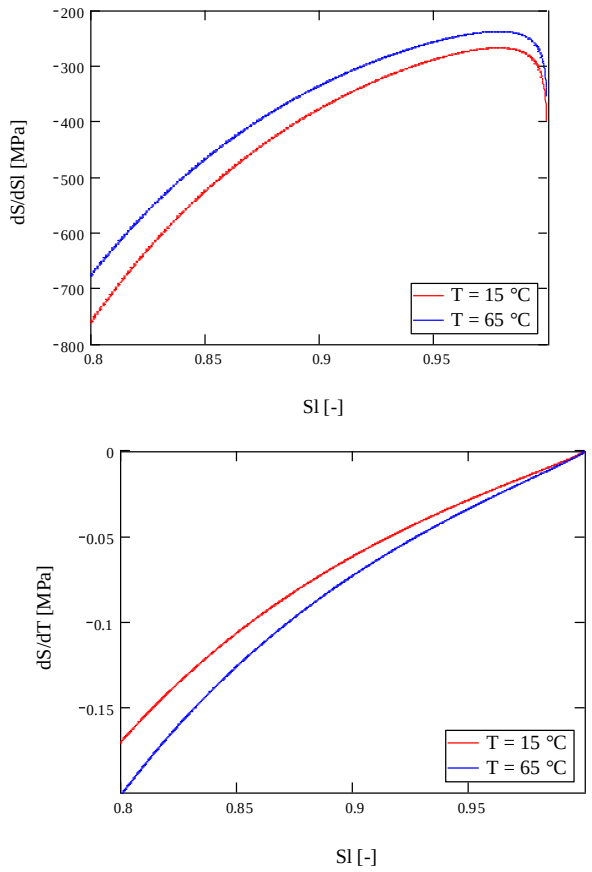

Figure A1 *The coefficients in (A7) plotted for* $S_l \in \{0.8, 1.0\}$ *at T = 15 °C and T = 65 °C.*

To obtain a expression for the water saturation rate, (A3) is operated on by the material time derivative. This gives

$$\dot{S}_l = \frac{1}{dV_p}(dV_w^{\,l}\dot{)} - \frac{S_l}{dV_p}(dV_p\dot{)} \tag{A8}$$

Using (A8) the water saturation rate can be calculated, which in turn can be translated into suction rate using (A7). The last term in (A8) is straight forward to express as

$$\frac{S_l}{dV_p}(dV_p\dot{)} = \frac{S_l}{e}\dot{e} \tag{A9}$$

When deriving an expression for the first term (A4) is operated on by the material derivative:

$$(dV_w^{\,l}\dot{)} = \frac{(dm_w^{\,l}\dot{)}}{\rho_l} - \frac{dV_w^{\,l}}{\rho_l}\dot{\rho}_l \tag{A10}$$

The obtained expression for the water saturation rate, inserting the results above and doing some rearrangements, reads

$$\dot{S}_l = \frac{1}{\rho_l e dV_s}(dm_w^{\,l}\dot{)} - \frac{S_l}{\rho_l}\dot{\rho}_l - \frac{S_l}{e}\dot{e} \tag{A11}$$

The liquid water mass can be expressed as, $dm_w^l = S_l \rho_l e\, dV_s$ and the corresponding rate, here divided by the solid volume, is approximated using

$$\frac{(dm_w^l)^{\cdot(i)}}{dV_s} \approx \frac{(dm_w^l)^{\cdot(i)}_{approx}}{dV_s} = 0.5\left(\frac{(S_l\rho_l e)^{(i)} - (S_l\rho_l e)^{(i-1)}}{t^i - t^{i-1}} + \frac{(S_l\rho_l e)^{(i+1)} - (S_l\rho_l e)^{(i)}}{t^{i+1} - t^i} \right) \quad \text{(A12)}$$

The two remaining rates in (A11) can be approximated using the differences in the variables in two succeeding time steps, here denoted by *i-1* and *i*, i.e.

$$\begin{aligned} \dot{\rho}_l^{(i)} &\approx \dot{\rho}_l^{(i)}{}_{approx} = 0.5\left(\frac{\rho_l^i - \rho_l^{i-1}}{t^i - t^{i-1}} + \frac{\rho_l^{i+1} - \rho_l^i}{t^{i+1} - t^i} \right) \\ \dot{e}^{(i)} &\approx \dot{e}^{(i)}{}_{approx} = 0.5\left(\frac{e^i - e^{i-1}}{t^i - t^{i-1}} + \frac{e^{i+1} - e^i}{t^{i+1} - t^i} \right) \end{aligned} \quad \text{(A13)}$$

Thus, when calculating the water saturation rate the expression

$$\dot{S}_l \approx \frac{1}{\rho_l e} \frac{(dm_w^l)^{\cdot}_{approx}}{dV_s} - \frac{S_l}{\rho_l} \dot{\rho}_{l\,approx} - \frac{S_l}{e} \dot{e}_{approx} \quad \text{(A14)}$$

is used.

The temperature rate present in (A7) can be approximated in the same way as the former rates, i.e.

$$\dot{T}^{(i)} \approx \dot{T}^{(i)}{}_{approx} = 0.5\left(\frac{T^i - T^{i-1}}{t^i - t^{i-1}} + \frac{T^{i+1} - T^i}{t^{i+1} - t^i} \right) \quad \text{(A15)}$$

Now, all quantities in (A7) are expressed in terms of Code_Bright output, and the origin of differences in suction rate can be investigated.